

Some Clustering-based Change-point Detection Methods Applicable to High Dimension, Low Sample Size Data

Trisha Dawn, Angshuman Roy, Alokesh Manna, Anil K. Ghosh

Theoretical Statistics and Mathematics Unit, Indian Statistical Institute, Kolkata, India.

Abstract

Detection of change-points in a sequence of high-dimensional observations is a very challenging problem, and this becomes even more challenging when the sample size (i.e., the sequence length) is small. In this article, we propose some change-point detection methods based on clustering, which can be conveniently used in such high dimension, low sample size situations. First, we consider the single change-point problem. Using k -means clustering based on some suitable dissimilarity measures, we propose some methods for testing the existence of a change-point and estimating its location. High-dimensional behavior of these proposed methods are investigated under appropriate regularity conditions. Next, we extend our methods for detection of multiple change-points. We carry out extensive numerical studies to compare the performance of our proposed methods with some state-of-the-art methods.

Keywords: Dissimilarity measure; Distribution-free property; Gini impurity index; High-dimensional consistency; Hypothesis testing; k -means clustering; Permutation test; Rand index.

1 Introduction

Detection of distributional changes in a sequence of multivariate observations is a classical problem in statistics and machine learning. In a sequence $\mathbf{X}_1 \sim F_1, \mathbf{X}_2 \sim F_2, \dots, \mathbf{X}_n \sim F_n$ of d -dimensional random variables, if $F_{\tau+1}$ ($1 \leq \tau < n$) differs from F_τ , the time-point τ is called a change-point. A sequence may have single or multiple change-points or it may not have any change-points at all. So, any method for change-point analysis has two major components: (i) the hypothesis testing part, where one tests whether the sequence has any change-points (ii) the estimation part, where one aims at finding the locations of the change-points if the answer to (i) is affirmative. If we assume that there is at most one change-point, it is called single change-point analysis, where we test the null hypothesis $\mathcal{H}_0 : F_1 = \dots = F_n$ against the alternative hypothesis $\mathcal{H}_1 : F_1 = \dots = F_\tau \neq F_{\tau+1} = \dots = F_n$ for some τ , and also estimate the change-point τ if \mathcal{H}_0 is rejected. In multiple change-point analysis, we allow the unknown number of change-points to be bigger than one.

Change-point analysis has its roots in statistical quality control (see, e.g., Girshick and Rubin, 1952; Page, 1954, 1955, 1957), and since then, several methods have been proposed in the literature. Parametric methods in the univariate set up (i.e., $d = 1$) include Sen and Srivastava (1975), Cox and Spjøtvoll (1982), Worsley (1986), James et al. (1987), Yao (1988), Lee (1995) and Chen and Gupta (1997, 1999). Several nonparametric methods (see, e.g., Bhattacharyya and Johnson, 1968; Pettitt, 1979; Wolfe and Schechtman, 1984; Csörgö and Horváth, 1987; Carlstein, 1988; Zou et al., 2014) are

also available. Chen and Gupta (2011) and Brodsky and Darkhovsky (2013) provide excellent reviews of univariate parametric and nonparametric methods, respectively.

For the multivariate data, notable works in the parametric regime include Sen and Srivastava (1973), Srivastava and Worsley (1986), James et al. (1992), Zhang et al. (2010) and Siegmund et al. (2011). However, these methods mainly detect the changes in mean in a sequence of independent Gaussian random vectors. Several nonparametric methods have been proposed as well. Nonparametric methods for detecting changes in location include those based on sparse linear projection (see, e.g., Aston and Kirch, 2014; Wang and Samworth, 2018), self-normalization (see, e.g., Shao and Zhang, 2010) and marginal rank statistics (see, e.g., Lung-Yut-Fong et al., 2015). These methods are applicable to high-dimensional data though Lung-Yut-Fong et al. (2015) needs the number of observations to be larger than the dimension. Aue et al. (2009), Avanesov and Buzun (2018) and Wang et al. (2021) proposed some methods for detecting changes in covariance matrices of high-dimensional random vectors.

Several nonparametric methods have been constructed for detecting the changes in distribution as well, and many of them can be used even in high dimension, low sample size situations. Chen and Zhang (2015) proposed some methods using graph-based two sample tests. In particular, they considered the tests based on minimum distance pairing (Rosenbaum, 2005), nearest neighbors (Schilling, 1986; Henze, 1988) and minimum spanning tree (Friedman and Rafsky, 1979). Some graph-based change-point detection methods were also proposed in Shi et al. (2017) and Sun et al. (2019). Matteson and James (2014) developed a method based on the energy statistic (see, e.g., Székely and Rizzo, 2013). Some kernel-based methods are also available in the literature (see, e.g., Desobry et al., 2005; Harchaoui et al., 2008; Li et al., 2015; Arlot et al., 2019). But as pointed out by Chen and Zhang (2015), the performance of these methods depends heavily on the choice of the kernel function and the associated tuning parameter called bandwidth. This problem becomes more prominent for high-dimensional data.

In this article, we propose some clustering-based methods for change-point analysis, which can be conveniently used for high-dimensional data, even when the dimension is much larger than the sample size. We know that there are two types of change-point problems: (i) offline, where the whole data set is available before the analysis and (ii) online, where observations arrive chronologically at the time of analysis. Here, we deal with the former one. The organization of the article is as follows.

In Section 2, we consider the single change-point problem and describe our clustering-based methods that use Rand index or impurity function for the detection of the change-point. However, these methods for change-point detection sometimes yield poor performance if we use clustering based on the Euclidean distance. So, we suggest using clustering based on a data-driven dissimilarity measure. In Section 3, we investigate the behavior of the resulting methods in high-dimensional asymptotic regime, where the dimension grows to infinity while the sample size remains fixed. Under appropriate regularity conditions, they turn out to be consistent when the change is in location or scale. For detecting changes outside the first two moments, we use a different dissimilarity function for clustering and change-point analysis. High-dimensional consistency of the resulting methods is also established under

suitable regularity conditions. In Section 4, we analyze some simulated and benchmark data sets to compare the performance of the proposed methods with some state-of-the-art methods. In Section 5, we extend our methods for multiple change-points detection and carry out numerical studies to evaluate their performance. Some additional issues related to our methods are discussed in Section 6. Finally, Section 7 contains a brief summary of the work and ends with some discussions on possible directions for future research. All proofs and mathematical details are given in the Appendix.

2 Methods for single change-point detection

To demonstrate how clustering helps in change-point detection, let us begin with some examples involving univariate data. Consider a sequence of 40 independent observations, where the first 20 observations come from the standard normal distribution, while the next 20 come from $N(\mu, 1)$. The left panel in Figure 1 shows the scatter plots of 40 observations for $\mu = 0$, $\mu = 4$ and $\mu = 2$, respectively, and the right panel shows the results of k -means clustering (with $k = 2$) on the corresponding data sets, where observations belonging to two clusters are marked using red and blue colors.

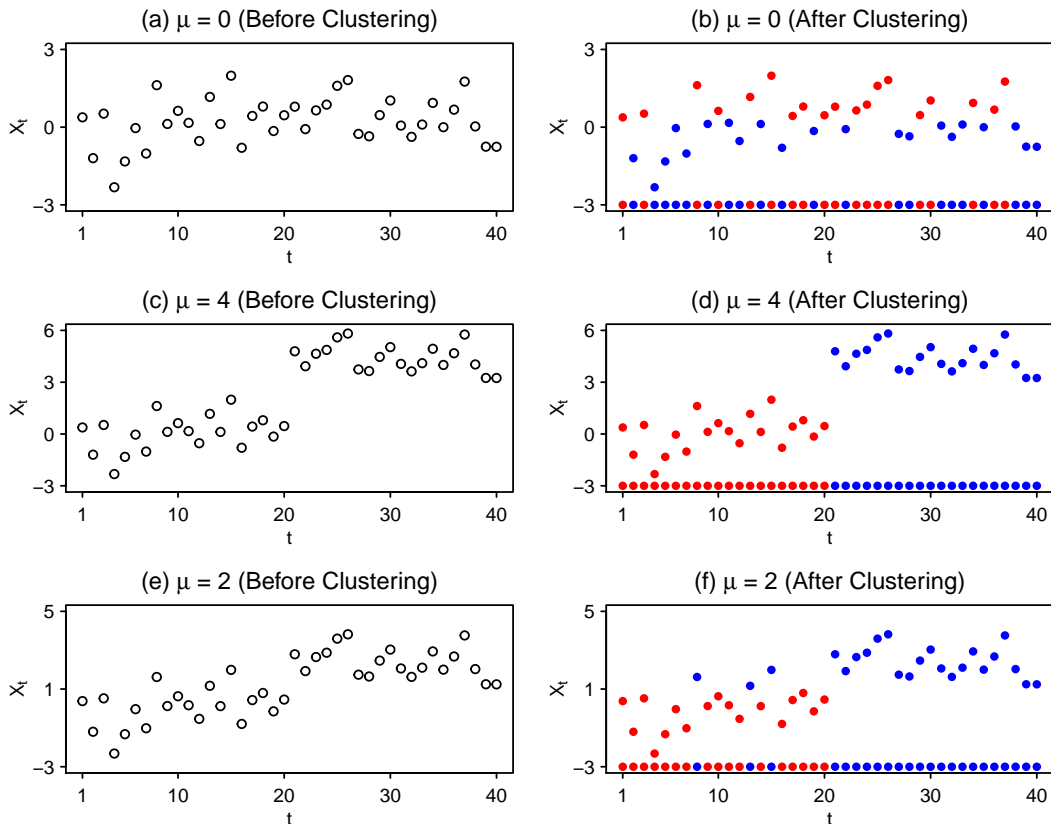


Figure 1: k -means clustering (with $k = 2$) of univariate data sets.

In the case of $\mu = 0$, when there are no change-points, clustering led to a random arrangement of red and blue colors (see Figure 1(b)). But in the case of $\mu = 4$, the first 20 observations were assigned to

one cluster and the rest to the other (see Figure 1(d)). As a result, we got a sequence of 20 red dots followed by 20 blue dots, which suggests the existence of a potential change-point at 20. However, the picture may not always be as clear as Figure 1(d). For instance, in the case of $\mu = 2$, clustering led to a sequence of red and blue dots, which does not look like a completely random sequence (see Figure 1(f)), but unlike Figure 1(d), the red and blue dots are not completely separable by a point on the x -axis. So, the exact location of the potential change-point is not very transparent from the sequence. To resolve this issue of identifying the potential change-point, now we propose two simple methods.

2.1 Method based on Rand index

Rand index (see Rand, 1971) was proposed to measure the dissimilarity between the outputs of two clustering algorithms. Let $\mathcal{C}(\mathbf{x}_i)$ be the cluster label ('0' or '1') assigned to the observation \mathbf{x}_i ($i = 1, 2, \dots, n$) by a clustering algorithm \mathcal{C} (e.g., the k -means algorithm with $k = 2$). Now for a fixed t ($1 \leq t < n$) let us consider a pseudo-clustering algorithm $\delta_t(\mathbf{x}_i) = \mathbb{I}\{i \leq t\}$, which puts $\{\mathbf{x}_1, \dots, \mathbf{x}_t\}$ in one cluster and $\{\mathbf{x}_{t+1}, \dots, \mathbf{x}_n\}$ in the other. We can use Rand index to measure the dissimilarity between these two clustering algorithms \mathcal{C} and δ_t . This is defined as

$$R(t) = \binom{n}{2}^{-1} \sum_{i < j} \mathbb{I}[\mathbb{I}\{\mathcal{C}(\mathbf{x}_i) = \mathcal{C}(\mathbf{x}_j)\} + \mathbb{I}\{\delta_t(\mathbf{x}_i) = \delta_t(\mathbf{x}_j)\} = 1].$$

Note that if t is actually a change-point, one would expect to have high similarity between δ_t and \mathcal{C} , or in other words, $R(t)$ is expected to be small. So, we can minimize $R(t)$ over $t = 1, 2, \dots, n - 1$ and consider $t_R^* = \arg \min R(t)$ as the potential change-point. Figure 2(a) shows the values of $R(t)$ for different values of t and three different choices of μ considered in Figure 1. We can see that both for $\mu = 2$ and $\mu = 4$, $R(t)$ was minimized at $t = 20$.

However, for this minimization, we do not need to compute $R(t)$ for all values of t . Lemma 1 shows that it is enough to check the values of t with $\mathcal{C}(\mathbf{x}_t) \neq \mathcal{C}(\mathbf{x}_{t+1})$. In the case of $\mu = 4$, there is only one t (i.e. $t = 20$) with this property. So, without any calculation, we can say that $t = 20$ is the minimizer. In the case of $\mu = 2$, however, we need to compute $R(t)$ for seven different choices of t including $t = 20$. In some rare cases, we may get multiple minimizers. In such situations, we can choose any one of them. However, in practice, one needs to detect the distributional changes as early as possible. So, from that perspective, it is better to choose the smallest of the minimizers as the potential change-point.

Lemma 1. *If $\mathcal{C}(\mathbf{x}_{t_0}) = \mathcal{C}(\mathbf{x}_{t_0+1})$, $R(t)$ cannot be minimized at $t = t_0$.*

The value of $R_{\min} = R(t_R^*)$ gives us an idea about the strength of evidence against \mathcal{H}_0 . In the case of $\mu = 4$, where we had a perfect separation of red and blue dots, this value was 0, but for $\mu = 2$, it was 0.1423. For $\mu = 0$, where we had no distributional changes, this turned out to be 0.5013. So, we can use R_{\min} as the test statistic and reject \mathcal{H}_0 when it is small. For finding the critical value, one can use the permutation test. Note that for any permutation of $\{\mathbf{x}_1, \mathbf{x}_2, \dots, \mathbf{x}_n\}$, the

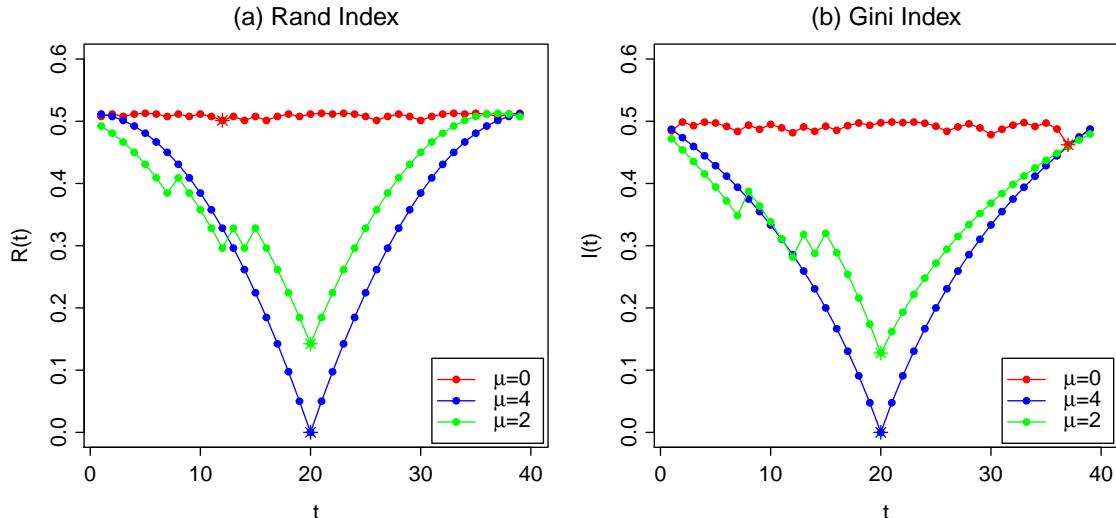


Figure 2: Rand index and Gini index for different choices of μ and t .

number of observations in each cluster (say, n_1 and n_2) remains the same, and a random permutation of $\{\mathbf{x}_1, \mathbf{x}_2, \dots, \mathbf{x}_n\}$ eventually leads to a random arrangement of n_1 red and n_2 blue dots. Since $\mathbf{x}_1, \mathbf{x}_2, \dots, \mathbf{x}_n$ are exchangeable under \mathcal{H}_0 , all these $\binom{n}{n_1}$ arrangements are equally likely. One can notice that R_{\min} is a function of the arrangement of red and blue dots. So, for any given n_1 and n_2 , its null distribution does not depend on the distribution of the sample observations. Because of this distribution-free property of R_{\min} , for different choices of n_1 and n_2 , cut-offs can be computed offline. For a level α -test, we find $r_{\alpha; n_1, n_2} = \max\{r : P_{\mathcal{H}_0}(R_{\min} < r \mid n_1, n_2) \leq \alpha\}$ and reject \mathcal{H}_0 if the observed value of R_{\min} is smaller than $r_{\alpha; n_1, n_2}$. Since R_{\min} is a discrete random variable, it may not always be possible to attain the upper bound α . To attain this upper bound and hence to improve the detection power of the change-point method, we use a randomized test using the test function $\phi_{\alpha; n_1, n_2}(z) = \mathbb{I}\{z < r_{\alpha; n_1, n_2}\} + \gamma \mathbb{I}\{z = r_{\alpha; n_1, n_2}\}$, where $\gamma \in [0, 1)$ is chosen such that $E_{\mathcal{H}_0}(\phi_{\alpha; n_1, n_2}(R_{\min}) \mid n_1, n_2) = P_{\mathcal{H}_0}(R_{\min} < r_{\alpha; n_1, n_2} \mid n_1, n_2) + \gamma P_{\mathcal{H}_0}(R_{\min} = r_{\alpha; n_1, n_2} \mid n_1, n_2) = \alpha$. If \mathcal{H}_0 is rejected, the potential change-point t_R^* is considered as an estimate of the change-point.

2.2 Method based on impurity function

We can borrow the idea from the classification tree literature (see, e.g., Breiman et al., 1984) to come up with another method based on impurity function. To construct a classification tree, we split a node into two child nodes such that the average impurity of the child nodes is minimum. For any fixed t ($1 \leq t < n$), let $p_1(t) = \sum_{i=1}^t \mathbb{I}\{\mathcal{C}(\mathbf{x}_i) = 0\}/t$ and $p_2(t) = \sum_{i=t+1}^n \mathbb{I}\{\mathcal{C}(\mathbf{x}_i) = 0\}/(n-t)$ be the proportions of observations in the first cluster (marked using red dots) among the first t and the last $(n-t)$ observations, respectively. So, if we divide the data set into two nodes consisting of observations $\{\mathbf{x}_1, \dots, \mathbf{x}_t\}$ and $\{\mathbf{x}_{t+1}, \dots, \mathbf{x}_n\}$, they will have impurity $\Phi(p_1(t))$ and $\Phi(p_2(t))$, respectively, where $\Phi : [0, 1] \rightarrow \mathbb{R}$ is an impurity function, which is concave and symmetric about 0.5. Since these two

nodes contain t and $n - t$ observations, respectively, the average impurity is given by

$$\mathcal{I}(t) = \frac{t}{n} \Phi(p_1(t)) + \frac{n-t}{n} \Phi(p_2(t)).$$

Note that concavity and symmetry of Φ ensure that $\Phi(p)$ is a decreasing function of $|p - 0.5|$ (see, e.g., Breiman et al., 1984). Gini index ($\Phi(p) = 2p(1 - p)$), entropy function ($\Phi(p) = -(1 - p) \log(1 - p) - p \log p$) and misclassification impurity ($\Phi(p) = \min\{p, 1 - p\}$) are some popular choices of the impurity function. Throughout this article, we use the Gini index for our numerical studies. If t is a true change-point, we expect $p_1(t)$ and $p_2(t)$ to close to 0 or 1, and as a result, $\mathcal{I}(t)$ is expected to be small. So, we can minimize $\mathcal{I}(t)$ over $t = 1, 2, \dots, n - 1$ and consider $t_{\mathcal{I}}^* = \arg \min \mathcal{I}(t)$ as the potential change-point. Figure 2(b) shows the values of $\mathcal{I}(t)$ (with $\Phi(p) = 2p(1 - p)$) for different values of t and three choices of μ considered in Figure 1. Both for $\mu = 2$ and $\mu = 4$, $\mathcal{I}(t)$ was minimized at $t = 20$. Here also, it is enough to minimize $\mathcal{I}(t)$ over the set $\{t : \mathcal{C}(\mathbf{x}_t) \neq \mathcal{C}(\mathbf{x}_{t+1})\}$. This is asserted by the following lemma.

Lemma 2. *If $\mathcal{C}(\mathbf{x}_{t_0}) = \mathcal{C}(\mathbf{x}_{t_0+1})$ and Φ is strictly concave, $\mathcal{I}(t)$ cannot be minimized at $t = t_0$.*

We can use $\mathcal{I}_{\min} = \mathcal{I}(t_{\mathcal{I}}^*)$ as the test statistic, and reject \mathcal{H}_0 for small values of it. Note that \mathcal{I}_{\min} is also a function of the arrangement of red and blue dots. So, given n_1 and n_2 (the number of observations in two clusters), it has the distribution-free property under \mathcal{H}_0 , and the cut-off can be computed offline. Since \mathcal{I}_{\min} is a discrete random variable, to make the size of the test exactly equal to α ($0 < \alpha < 1$), we may need to use a randomized test with the randomization at the boundary point as before.

Though we have used some univariate examples for the demonstration of our proposed methods, from our description, it is quite transparent that these methods can be conveniently used for high-dimensional data. In the next section, we investigate their performance in high dimension, low sample size situations.

3 Behavior of the proposed methods for high-dimensional data

Consider a change-point problem, where we have the first 20 observations from $N_{100}(\mathbf{0}_{100}, \sigma_1^2 \mathbf{I}_{100})$ and the next 20 from $N_{100}(\mu \mathbf{1}_{100}, \sigma_2^2 \mathbf{I}_{100})$. Here $N_d(\boldsymbol{\mu}, \boldsymbol{\Sigma})$ denotes a d -dimensional normal distribution with the mean $\boldsymbol{\mu}$ and the dispersion matrix $\boldsymbol{\Sigma}$, $\mathbf{0}_d = (0, 0, \dots, 0)^\top$ and $\mathbf{1}_d = (1, 1, \dots, 1)^\top$ are d -dimensional vectors with all elements equal to 0 and 1, respectively, and \mathbf{I}_d is the $d \times d$ identity matrix. We used k -means clustering (with $k = 2$) based on the Euclidean distance, and then the methods based on Rand index and Gini index (with associate level $\alpha = 0.05$) were used for change-point detection. This experiment was repeated 100 times, and the results are reported in Figure 3. When we used $\mu = 0.7$ and $\sigma_1 = \sigma_2 = 1$ (call it Example-A), both of these methods selected the true change-point on almost all occasions (see Figure 3(a)). But we observed a different picture when the value of σ_2 was changed to 2 keeping μ and σ_1 unchanged (call it Example B). In that example, the success rate (i.e., the proportion of times the true change-point is detected) of these two methods dropped down significantly (see Figure 3(b)). The methods based on Gini index and Rand index detected the true change-point in 57% and

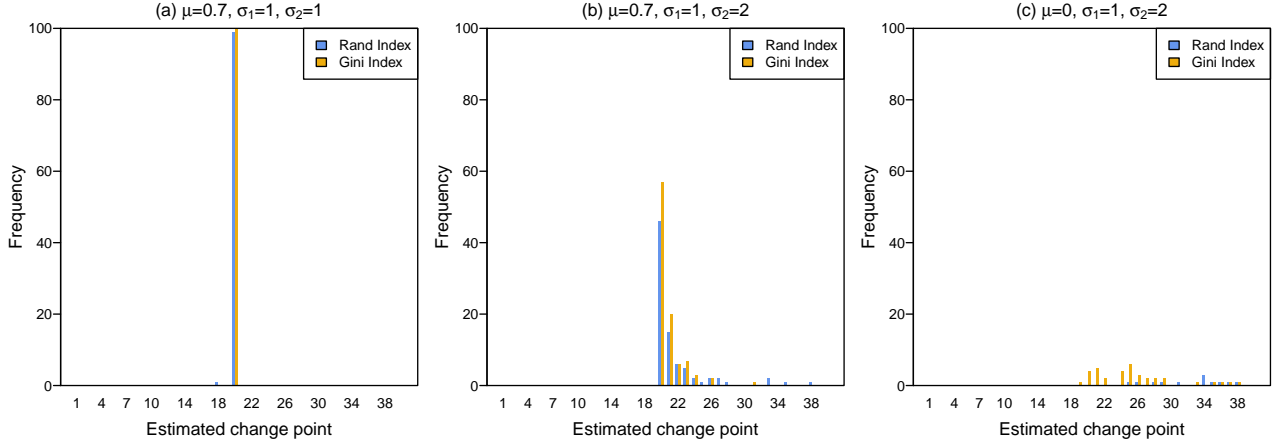


Figure 3: Frequency distribution of the estimated change-points in Examples A-C when the k -means algorithm (with $k = 2$) based on the Euclidean distance was used for clustering.

46% cases, respectively. Their performance was even worse when we used $\mu = 0$, $\sigma_1 = 1$ and $\sigma_2 = 2$ (call it Example C). The method based on Gini index (respectively, Rand index) detected the true change-point in only 4 (repectively, 0) out of 100 cases (see Figure 3(c)).

A careful theoretical investigation reveals the reason behind these surprising results. Consider n independent random vectors $\mathbf{X}_1, \dots, \mathbf{X}_\tau \sim N_d(\mathbf{0}_d, \sigma_1^2 \mathbf{I}_d)$, $\mathbf{X}_{\tau+1}, \dots, \mathbf{X}_n \sim N_d(\mu \mathbf{1}_d, \sigma_2^2 \mathbf{I}_d)$. Note that for $i, j \leq \tau$, $d^{-1} \|\mathbf{X}_i - \mathbf{X}_j\|^2$, being an average of d independent and identically distributed (i.i.d.) random variables, converges almost surely (a.s.) to $2\sigma_1^2$ as d grows to infinity. Similarly, as $d \rightarrow \infty$, we have $d^{-1} \|\mathbf{X}_i - \mathbf{X}_j\|^2 \xrightarrow{a.s.} 2\sigma_2^2$ for $i, j > \tau$ and $d^{-1} \|\mathbf{X}_i - \mathbf{X}_j\|^2 \xrightarrow{a.s.} \mu^2 + \sigma_1^2 + \sigma_2^2$ for $i \leq \tau < j$ or $j \leq \tau < i$. Therefore, in Example A, where we have $\mu^2 = 0.49$ and $\sigma_1^2 = \sigma_2^2 = 1$, an observation from $N(\mathbf{0}_d, \mathbf{I}_d)$ has its neighbor from the same distribution with probability tending to 1. The same is true for the observations from $N(\mu \mathbf{1}_d, \mathbf{I}_d)$ as well. Note that given a set of observations $\mathbf{x}_1, \dots, \mathbf{x}_n$, the usual k -means (with $k = 2$) algorithm aims at finding two clusters C_1 and C_2 with centers \mathbf{m}_1 and \mathbf{m}_2 such that $\lambda(C_1, C_2) = \sum_{j=1}^2 \sum_{i: \mathbf{x}_i \in C_j} \|\mathbf{x}_i - \mathbf{m}_j\|^2 = \sum_{j=1}^2 \sum_{(i,i'): \mathbf{x}_i, \mathbf{x}_{i'} \in C_j} \frac{1}{2|C_j|} \|\mathbf{x}_i - \mathbf{x}_{i'}\|^2$ is minimized. Here $|C_j|$ ($j = 1, 2$) denotes the number of observations in C_j (clearly, $|C_1| + |C_2| = n$). Now, from our above discussion it is quite clear that in Example A, $\lambda(C_1, C_2)$ gets minimized when the first 20 observations are assigned to one cluster and the rest to the other (see Lemma 3(i) and its proof in Appendix for mathematical details). As a result, the change-point was correctly estimated. But in Example B, where we have $\mu^2 = 0.49$, $\sigma_1^2 = 1$ and $\sigma_2^2 = 4$, an observation from $N_d(\mu \mathbf{1}_d, \sigma_2^2 \mathbf{I}_d)$ has neighbor its neighbor from $N_d(\mathbf{0}_d, \sigma_1^2 \mathbf{I}_d)$ with probability converging to 1. Because of this violation of neighborhood structure, the k -means algorithm could not perform well, and that affected the performance of our change-point detection methods. We have a similar situation in Example C as well. In fact, in this case with $\mu^2 = 0$, one can show that the k -means algorithm leads to one cluster consisting of a single observation, while the other containing the rest (see Lemma 3(ii) and its proof in Appendix). So, the poor performance of the proposed method was quite expected.

Violation of this neighborhood structure in high dimension is quite well-known for Euclidean and fractional distances (see, e.g., Francois et al., 2007; Radovanovic et al., 2010), and researchers have investigated its adverse effects on supervised and unsupervised classification (see, e.g., Hall et al., 2005; Borysov et al., 2014; Sarkar and Ghosh, 2020). Note that the Euclidean distance between two points does not depend on the mass distribution of the data cloud. To extract information from the mass distribution, several data-based dissimilarity measures have been proposed in the literature (see, e.g., Ting et al., 2016; Aryal et al., 2017). But, due to sparsity of the data cloud, many of them are not well-suited for high-dimensional data. In this article, we use the dissimilarity measure used by Pal et al. (2016) to take care of this problem. For a data set consisting of n observations $\{\mathbf{x}_1, \mathbf{x}_2, \dots, \mathbf{x}_n\}$, they defined the dissimilarity between two observations \mathbf{x}_i and \mathbf{x}_j as

$$\delta_0(\mathbf{x}_i, \mathbf{x}_j) = \frac{1}{n-2} \sum_{k=1, k \neq i, j}^n \left| \|\mathbf{x}_i - \mathbf{x}_k\| - \|\mathbf{x}_j - \mathbf{x}_k\| \right|.$$

One can check that δ_0 is a pseudometric, which is non-negative, symmetric in its arguments and satisfies the triangle inequality. If $\mathbf{X}_1, \dots, \mathbf{X}_\tau \stackrel{i.i.d.}{\sim} N_d(\mathbf{0}_d, \sigma_1^2 \mathbf{I}_d)$ and $\mathbf{X}_{\tau+1}, \dots, \mathbf{X}_n \stackrel{i.i.d.}{\sim} N_d(\mu \mathbf{1}_d, \sigma_2^2 \mathbf{I}_d)$, from our above discussion, it is clear that for $i, j \leq \tau$ or $i, j > \tau$, as d increases to infinity, $d^{-1/2}(n-2)\delta_0(\mathbf{X}_i, \mathbf{X}_j)$ converges to 0 almost surely, but for $i \leq \tau < j$ or $j \leq \tau < i$, it converges almost surely to $(\tau-1)|\sqrt{\mu^2 + \sigma_1^2 + \sigma_2^2} - \sigma_1\sqrt{2}| + (n-\tau-1)|\sqrt{\mu^2 + \sigma_1^2 + \sigma_2^2} - \sigma_2\sqrt{2}|$, which is positive unless $\mu^2 = 0$ and $\sigma_1^2 - \sigma_2^2 = 0$ (follows from Lemma 4 in Appendix). Therefore, unlike the Euclidean distance, δ_0 preserves the neighborhood structure in high dimensions. So, it is more reasonable to use k -means clustering based on δ_0 , where one aims at finding the clusters C_1 and C_2 such that $\lambda^*(C_1, C_2) = \sum_{j=1}^2 \frac{1}{2|C_j|} \sum_{(i, i'): \mathbf{x}_i, \mathbf{x}_{i'} \in C_j} \delta_0^2(\mathbf{x}_i, \mathbf{x}_{i'})$ is minimized. Like the usual k -means clustering algorithm, we start with two initial clusters and update them iteratively. Note that the squared Euclidean distance between an observation \mathbf{x}_i ($i = 1, 2, \dots, n$) and \mathbf{m}_j , the center of cluster C_j ($j = 1, 2$), can be expressed as $\|\mathbf{x}_i - \mathbf{m}_j\|^2 = \frac{1}{|C_j|} \sum_{k: \mathbf{x}_k \in C_j} \|\mathbf{x}_i - \mathbf{x}_k\|^2 - \frac{1}{2|C_j|^2} \sum_{(k, \ell): \mathbf{x}_k, \mathbf{x}_\ell \in C_j} \|\mathbf{x}_k - \mathbf{x}_\ell\|^2$. So, at any stage, we compute $d_0(\mathbf{x}_i, C_j) = \frac{1}{|C_j|} \sum_{k: \mathbf{x}_k \in C_j} \delta_0^2(\mathbf{x}_i, \mathbf{x}_k) - \frac{1}{2|C_j|^2} \sum_{(k, \ell): \mathbf{x}_k, \mathbf{x}_\ell \in C_j} \delta_0^2(\mathbf{x}_k, \mathbf{x}_\ell)$ for $j = 1, 2$ and assign \mathbf{x}_i to the first (respectively, second) cluster if and only if $d_0(\mathbf{x}_i, C_1) < d_0(\mathbf{x}_i, C_2)$ (respectively, $d_0(\mathbf{x}_i, C_1) > d_0(\mathbf{x}_i, C_2)$). We do it for all $i = 1, 2, \dots, n$, and the process is repeated until there are no changes in C_1 and C_2 or the maximum number of iterations is reached. When we used the k -means algorithm based on δ_0 for clustering, the methods based on Rand index and Gini index (henceforth referred to as RI₀ and GI₀) had excellent performance in Examples A-C (see Figure 4). They correctly estimated the true change-point in almost all occasions.

Ahn et al. (2012) also developed a clustering algorithm for high dimension, low sample size data. But their method based on maximum data piling distance performs poorly for high-dimensional scale problems (see, e.g., Sarkar and Ghosh, 2020). Sparse subspace clustering algorithms (see, e.g., Elhamifar and Vidal, 2013) assume that the observations from different populations lie in different low dimensional linear subspaces. They yield poor performance when this is not the case.

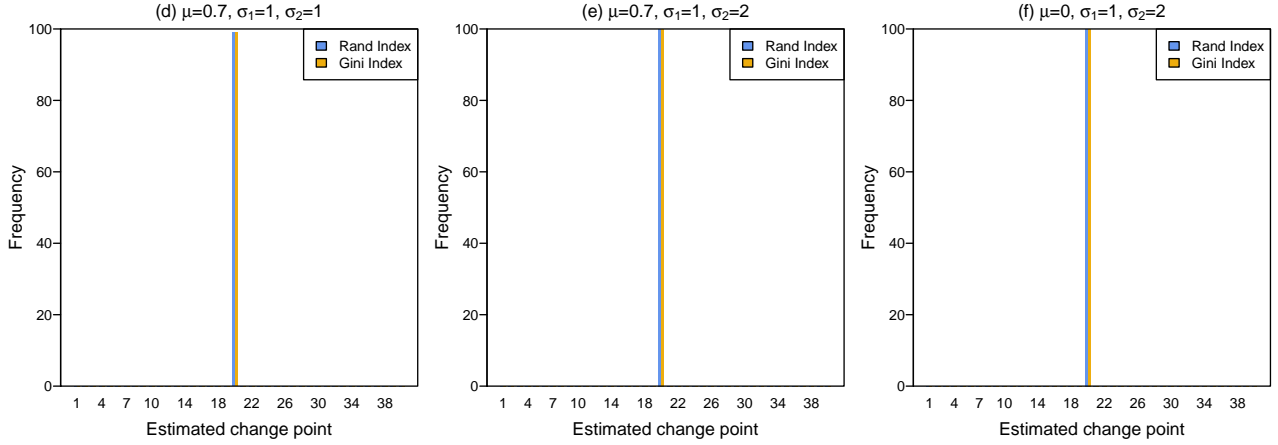


Figure 4: Frequency distribution of the estimated change-points in Examples A-C when the k -means algorithm (with $k = 2$) based on δ_0 was used for clustering.

3.1 High-dimensional behavior of RI_0 and GI_0

To properly understand the high-dimensional behavior of RI_0 and GI_0 , we carry out further investigation. For this investigation, we assume that $\mathbf{X}_1, \mathbf{X}_2, \dots, \mathbf{X}_\tau \stackrel{i.i.d.}{\sim} G_1$ and $\mathbf{X}_{\tau+1}, \mathbf{X}_{\tau+2}, \dots, \mathbf{X}_n \stackrel{i.i.d.}{\sim} G_2$, where G_i has the mean vector $\boldsymbol{\mu}_{i,d}$ and the scatter matrix $\boldsymbol{\Sigma}_{i,d}$ ($i = 1, 2$). We also assume that

(A1) For two independent random vectors $\mathbf{X} = (X^{(1)}, \dots, X^{(d)})^\top \sim G_r$ and $\mathbf{Y} = (Y^{(1)}, \dots, Y^{(d)})^\top \sim G_s$ ($r, s = 1, 2$), $d^{-1}[\|\mathbf{X} - \mathbf{Y}\|^2 - E\|\mathbf{X} - \mathbf{Y}\|^2] \xrightarrow{P} 0$ as $d \rightarrow \infty$.

For $\mathbf{X}_i = (X_i^{(1)}, \dots, X_i^{(d)})^\top \sim G_r$ and $\mathbf{X}_j = (X_j^{(1)}, \dots, X_j^{(d)})^\top \sim G_s$ ($r, s = 1, 2$), (A1) says that the weak law of large number (WLLN) holds for the sequence $\{(X_i^{(q)} - X_j^{(q)})^2 : q \geq 1\}$. If the coordinate variables are i.i.d. with finite second moments (like Examples A-C), WLLN holds for this sequence. To have WLLN for non-identically distributed dependent random variables, we need some extra conditions. For instance, WLLN holds if the coordinate variables have uniformly bounded fourth moments with $\sum_{q,r} \text{Corr}((X_i^{(q)} - X_j^{(q)})^2, (X_i^{(r)} - X_j^{(r)})^2) = o(d^2)$ (see, e.g., Pal et al., 2016). For sequence data, this holds if the sequence is m -dependent or it has the rho-mixing property (see, e.g., Hall et al., 2005). This assumption was used by Hall et al. (2005) for investigating high-dimensional behavior of some popular classifiers. Jung and Marron (2009) considered similar assumptions for studying their estimated principal component directions in high dimensions. Under these conditions, high-dimensional consistency of our proposed change-point detection methods is given by the following theorem.

Theorem 1. *Suppose that $\mathbf{X}_1, \dots, \mathbf{X}_\tau \stackrel{i.i.d.}{\sim} G_1$ and $\mathbf{X}_{\tau+1}, \dots, \mathbf{X}_n \stackrel{i.i.d.}{\sim} G_2$, where $1 < \tau < n - 1$, and G_1 and G_2 satisfy (A1). Also assume that as $d \rightarrow \infty$, (i) $d^{-1}\|\boldsymbol{\mu}_{1,d} - \boldsymbol{\mu}_{2,d}\|^2 \rightarrow \mu^2$ and (ii) $d^{-1}\text{tr}(\boldsymbol{\Sigma}_{i,d}) \rightarrow \sigma_i^2$ for $i = 1, 2$. If $\mu^2 > 0$ or $\sigma_1^2 \neq \sigma_2^2$, and $\binom{n}{\tau} > 2/\alpha$, then for RI_0 and GI_0 with associated level α ($0 < \alpha < 1$), the probabilities of detecting the true-change point τ converge to 1 as d grows to infinity.*

The condition $\binom{n}{\tau} > 2/\alpha$ holds if n is not very small. If the change-point is at the center, for $\alpha = 0.05$, it is enough to have 8 observations. We need slightly more observations as the change-point moves towards the boundary. In the extreme cases (i.e., $\tau = 2$ or $n - 2$), we need 10 observations. Hall et al. (2005) assumed conditions (i) and (ii) of Theorem 1 for studying high-dimensional behavior of some classifiers. Note that they hold in Examples A-C. Pal et al. (2016) also assumed these conditions and proved the perfect classification property of their nearest neighbor classifiers when $\mu^2 > 0$ or $|\sigma_1^2 - \sigma_2^2| > 0$. Theorem 1 proves the consistency of our methods under similar conditions.

Note that " $\mu^2 = \lim_{d \rightarrow \infty} \frac{1}{d} \|\boldsymbol{\mu}_{1,d} - \boldsymbol{\mu}_{2,d}\|^2 > 0$ or $|\sigma_1^2 - \sigma_2^2| = \lim_{d \rightarrow \infty} d^{-1} [\text{tr}(\boldsymbol{\Sigma}_{1,d}) - \text{tr}(\boldsymbol{\Sigma}_{2,d})] > 0$ " implies that $\|\boldsymbol{\mu}_{1,d} - \boldsymbol{\mu}_{2,d}\|^2$ or $[\text{tr}(\boldsymbol{\Sigma}_{1,d}) - \text{tr}(\boldsymbol{\Sigma}_{2,d})]$ grows linearly with d . However, in some cases, it is possible to relax this condition. Let $O(v_{r,s,d}^2)$ be the asymptotic order of $\text{Var}(\|\mathbf{X}_i - \mathbf{X}_j\|^2)$ when $\mathbf{X}_i \sim G_r$ and $\mathbf{X}_j \sim G_s$ ($r, s = 1, 2$) are independent. Define $v_d^2 = \max\{v_{1,1,d}^2, v_{1,2,d}^2, v_{2,2,d}^2\}$. For instance, if the coordinate variables in G_1 and G_2 are independent (like Examples A-C) or m -dependent, we have $v_d^2 = d$ or $v_d = d^{1/2}$. If v_d is of smaller asymptotic order than d (note that under (A1), it is reasonable to assume that v_d^2/d^2 or v_d/d converges to 0 as $d \rightarrow \infty$), for the high-dimensional consistency of our proposed methods, we only need either $\|\boldsymbol{\mu}_{1,d} - \boldsymbol{\mu}_{2,d}\|^2$ or $|\text{tr}(\boldsymbol{\Sigma}_{1,d}) - \text{tr}(\boldsymbol{\Sigma}_{2,d})|$ to be of higher asymptotic order than v_d (see Theorem 2). So, in the case of independent or m -dependent coordinate variables, it is enough to have the divergence of $d^{-1/2} \|\boldsymbol{\mu}_{1,d} - \boldsymbol{\mu}_{2,d}\|^2$ or $d^{-1/2} |\text{tr}(\boldsymbol{\Sigma}_{1,d}) - \text{tr}(\boldsymbol{\Sigma}_{2,d})|$. Unlike Theorem 1, we do not need $d^{-1} \|\boldsymbol{\mu}_{1,d} - \boldsymbol{\mu}_{2,d}\|^2$ or $d^{-1} |\text{tr}(\boldsymbol{\Sigma}_{1,d}) - \text{tr}(\boldsymbol{\Sigma}_{2,d})|$ to converge to a positive constant.

Theorem 2. *Suppose that $\mathbf{X}_1, \dots, \mathbf{X}_\tau \stackrel{i.i.d.}{\sim} G_1$ and $\mathbf{X}_{\tau+1}, \dots, \mathbf{X}_n \stackrel{i.i.d.}{\sim} G_2$, where G_1 and G_2 satisfy (A1) and $1 < \tau < n - 1$. Let $\boldsymbol{\mu}_{i,d}$ and $\boldsymbol{\Sigma}_{i,d}$ be the mean vector and the dispersion matrix of G_i ($i = 1, 2$). Also assume that $\liminf_{d \rightarrow \infty} \min\{\text{tr}(\boldsymbol{\Sigma}_{1,d}), \text{tr}(\boldsymbol{\Sigma}_{2,d})\}/v_d > 0$. If $\|\boldsymbol{\mu}_{1,d} - \boldsymbol{\mu}_{2,d}\|^2/v_d \rightarrow \infty$ or $|\text{tr}(\boldsymbol{\Sigma}_{1,d}) - \text{tr}(\boldsymbol{\Sigma}_{2,d})|/v_d \rightarrow \infty$ as $d \rightarrow \infty$, and $\binom{n}{\tau} > 2/\alpha$, then for RI_0 and GI_0 with associated level α ($0 < \alpha < 1$), the probabilities of detecting the true change-point τ converge to 1 as d grows to infinity.*

Note that if G_1 and G_2 differ (either in locations or in scales) only in d^β ($0 < \beta < 1$) many coordinates, $d^{-1} \|\boldsymbol{\mu}_{1,d} - \boldsymbol{\mu}_{2,d}\|^2$ and $d^{-1} |\text{tr}(\boldsymbol{\Sigma}_{1,d}) - \text{tr}(\boldsymbol{\Sigma}_{2,d})|$ both converge to 0 as d increases. To study the high-dimensional performance of RI_0 and GI_0 for such sparse signals, we consider three examples. In each of these examples, we take $G_1 = N_d(\mathbf{0}_d, \mathbf{I}_d)$, while G_2 differs from G_1 in $d_* = \lfloor d^{2/3} \rfloor$ many coordinates. In the first example (location problem), G_2 is multivariate normal with mean vector $(\mathbf{1}_{d_*}^\top, \mathbf{0}_{d-d_*}^\top)^\top$ and the dispersion matrix \mathbf{I}_d . In the second example (location-scale problem), it has the same mean vector, but a diagonal dispersion matrix with the first d_* elements equal to 3 and the rest equal to 1. In the third example (scale problem), it has the same dispersion matrix as in the second example, but the mean vector is $\mathbf{0}_d$. Note that in these examples, either $d^{-1/2} \|\boldsymbol{\mu}_{1,d} - \boldsymbol{\mu}_{2,d}\|^2$ or $d^{-1/2} |\text{tr}(\boldsymbol{\Sigma}_{1,d}) - \text{tr}(\boldsymbol{\Sigma}_{2,d})|$ diverges to infinity as d increases.

For each example, we generated the first 20 observations from G_1 and the next 20 from G_2 . We carried out these experiments for different choices of d and in each case, the experiment was repeated 100 times to assess the performance of RI_0 and GI_0 . Figure 5 shows the proportion of times the true change-point

was detected by these methods. In each example, these proportions gradually climbed up to 1 as the dimension increased. This is consistent with the result reported in Theorem 2.

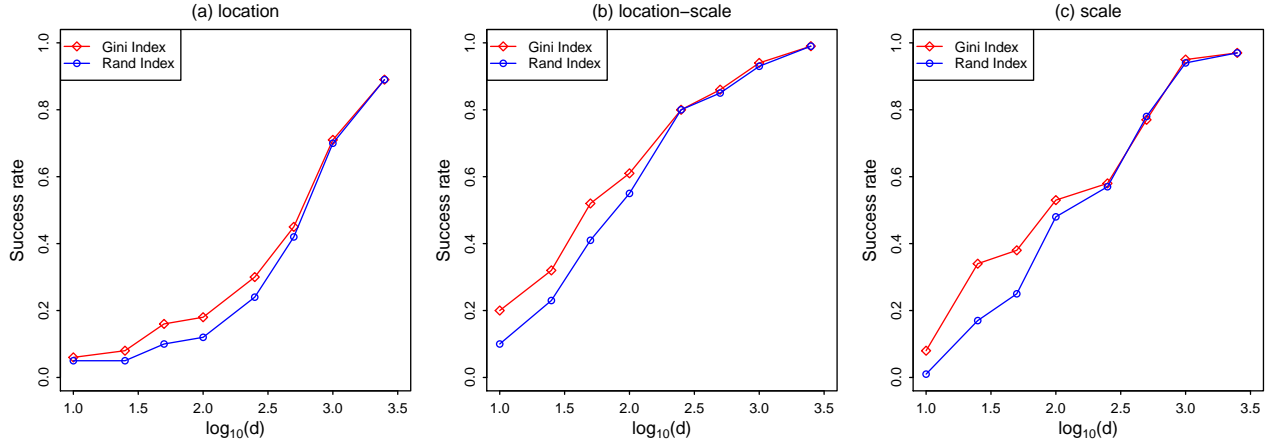


Figure 5: Success rates of RI_0 and GI_0 under sparse signals as d varies.

Theorems 1 and 2 show that our methods can successfully detect the change-point even when the two distributions have the same location, but the traces of their dispersion matrices differ. Now, one may be curious to know what happens if the two dispersion matrices have the same trace, but they differ in their diagonal elements. For this investigation, we consider an example (call it Example D), where we generate the first 20 observations from $N_{200}(\mathbf{0}_{200}, \Sigma_1)$ and the next 20 from $N_{200}(\mathbf{0}_{200}, \Sigma_2)$. Here Σ_1 (respectively, Σ_2) is a 200×200 diagonal matrix with the first 100 diagonal elements equal to 1 (respectively, 3) and the rest equal to 3 (respectively, 1). This experiment is repeated 100 times as before to assess the performance of the proposed tests. Unfortunately, RI_0 and GI_0 both performed poorly in this example (see Figure 6(a)). We had the same experience when instead of δ_0 , the usual Euclidean distance was used for clustering. In this example, though each coordinate variable provides some signal against \mathcal{H}_0 , that signal is not reflected in pairwise Euclidean distances. One can check that

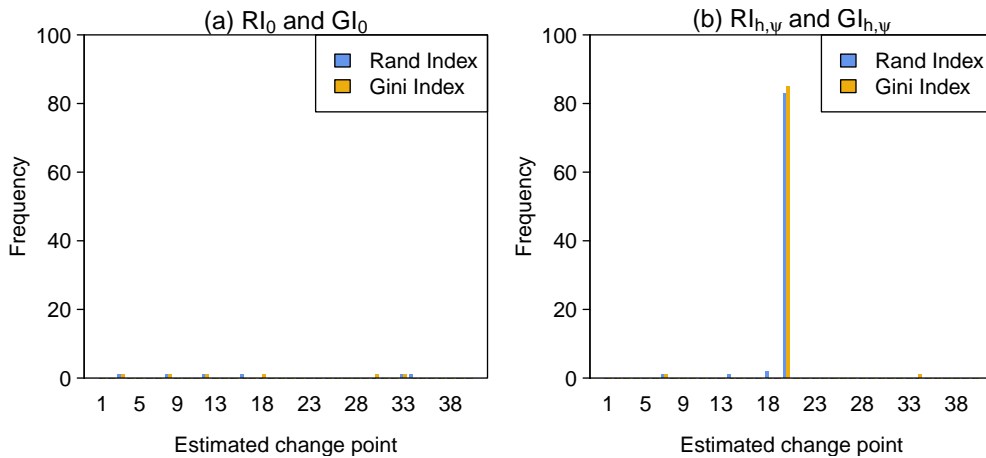


Figure 6: Frequency distribution of change-points estimated by (a) RI_0 and GI_0 and (b) $RI_{h,\psi}$ and $GI_{h,\psi}$ with $h(t) = t$ and $\psi(t) = 1 - e^{-\sqrt{t}}$ in Example D.

here all pairwise Euclidean distances converge to the same constant. So, δ_0 , which is constructed using pairwise Euclidean distances, was not helpful in detecting the differences between the two distributions. As a result, the k -means clustering algorithm and the associated change-point methods failed to have satisfactory performance.

To take care of this problem, we consider a class of distance function of the form

$$\rho_{h,\psi}(\mathbf{x}_1, \mathbf{x}_2) = h\left\{\frac{1}{d} \sum_{q=1}^d \psi\left((\mathbf{x}_1^{(q)} - \mathbf{x}_2^{(q)})^2\right)\right\}$$

and use it to construct a data-based dissimilarity function $\delta_{h,\psi}$. For a data cloud $\{\mathbf{x}_1, \mathbf{x}_2, \dots, \mathbf{x}_n\}$ consisting of n observations, the dissimilarity between \mathbf{x}_i and \mathbf{x}_j is given by

$$\delta_{h,\psi}(\mathbf{x}_i, \mathbf{x}_j) = \frac{1}{n-2} \sum_{k=1, k \neq i, j}^n \left| \rho_{h,\psi}(\mathbf{x}_i, \mathbf{x}_k) - \rho_{h,\psi}(\mathbf{x}_j, \mathbf{x}_k) \right|.$$

Here h and ψ are two monotonically increasing continuous function with $h(0) = \psi(0) = 0$. Note that for $p \geq 1$, using $\psi(t) = t^{p/2}$ and $h(t) = t^{1/p}$, one gets a scaled version of the ℓ_p -distance. In particular, for $p = 2$, we get $\rho_{h,\psi}(\mathbf{x}_i, \mathbf{x}_j) = d^{-1/2} \|\mathbf{x}_i - \mathbf{x}_j\|$ and $\delta_{h,\psi}(\mathbf{x}_i, \mathbf{x}_j) = d^{-1/2} \delta_0(\mathbf{x}_i, \mathbf{x}_j)$. We choose h and ψ such that $\rho_{h,\psi}$ is a distance function, and in such cases $\delta_{h,\psi}$ turns out to be a semi-metric. For instance one can take $h(t) = t$ and $\psi(t) = 1 - e^{-\sqrt{t}}$. When we used this dissimilarity measure for clustering, the resulting change-point detection methods had excellent performance in Example D (see Figure 6(b)). This gives us the motivation to investigate the high-dimensional behavior of the dissimilarity function $\delta_{h,\psi}$ and the resulting change-point detection methods based on Rand index and Gini index (henceforth referred to as $\text{RI}_{h,\psi}$ and $\text{GI}_{h,\psi}$, respectively) in the following subsection.

3.2 High-dimensional behavior of $\text{RI}_{h,\psi}$ and $\text{GI}_{h,\psi}$

For investigating the high-dimensional behavior of $\delta_{h,\psi}$, first we make an assumption similar to (A1), which is stated below.

(A2) For two independent random vectors $\mathbf{X} = (X^{(1)}, \dots, X^{(d)})^\top \sim G_r$ and $\mathbf{Y} = (Y^{(1)}, \dots, Y^{(d)})^\top \sim G_s$ ($r, s = 1, 2$), $d^{-1} \left[\sum_{q=1}^d \psi\left((X^{(q)} - Y^{(q)})^2\right) - E\left\{ \sum_{q=1}^d \psi\left((X^{(q)} - Y^{(q)})^2\right) \right\} \right] \xrightarrow{P} 0$ as $d \rightarrow \infty$.

For $\mathbf{X}_1, \dots, \mathbf{X}_\tau \sim G_1$ and $\mathbf{X}_{\tau+1}, \dots, \mathbf{X}_n \sim G_2$, let us define $\theta_{\psi,1}^{(q)}, \theta_{\psi,2}^{(q)}$ and $\theta_{\psi,3}^{(q)}$ ($q = 1, 2, \dots, d$) as the expectation of $\psi\left((X_i^{(q)} - X_j^{(q)})^2\right)$ for $i, j \leq \tau$, $i, j > \tau$ and $i \leq \tau < j$, respectively. If we consider h to be uniformly continuous and define $\tilde{\theta}_{\psi,1,d} = \frac{1}{d} \sum_{q=1}^d \theta_{\psi,1}^{(q)}$ (continuity of h is enough if we assume that $\tilde{\theta}_{\psi,1,d}$ has a limit as d tends to infinity), one can show that for $i, j \leq \tau$, $|\rho_{h,\psi}(\mathbf{X}_i, \mathbf{X}_j) - h(\tilde{\theta}_{\psi,1,d})| \xrightarrow{P} 0$. Similarly, for $i, j > \tau$ and $i \leq \tau < j$, we have $|\rho_{h,\psi}(\mathbf{X}_i, \mathbf{X}_j) - h(\tilde{\theta}_{\psi,2,d})| \xrightarrow{P} 0$ and $|\rho_{h,\psi}(\mathbf{X}_i, \mathbf{X}_j) - h(\tilde{\theta}_{\psi,3,d})| \xrightarrow{P} 0$, respectively, where $\tilde{\theta}_{\psi,r,d} = \frac{1}{d} \sum_{q=1}^d \theta_{\psi,r}^{(q)}$ for $r = 2, 3$. Using these results, one can show that $\delta_{h,\psi}(\mathbf{X}_i, \mathbf{X}_j) \xrightarrow{P} 0$ for $i, j \leq \tau$ and $i, j > \tau$. Now, we need to investigate the asymptotic behavior

of $\delta_{h,\psi}(\mathbf{X}_i, \mathbf{X}_j)$ for $i \leq \tau < j$. It can be shown that as $d \rightarrow \infty$, $|\delta_{h,\psi}(\mathbf{X}_i, \mathbf{X}_j) - \tilde{\delta}_{h,\psi,d}| \xrightarrow{P} 0$, where $(n-2)\tilde{\delta}_{h,\psi,d} = (\tau-1)|h(\tilde{\theta}_{\psi,1,d}) - h(\tilde{\theta}_{\psi,3,d})| + (n-\tau-1)|h(\tilde{\theta}_{\psi,3,d}) - h(\tilde{\theta}_{\psi,2,d})|$. If ψ has a non-constant completely monotone derivative, we have $\mathcal{E}_\psi(q) = 2\theta_{\psi,3}(q) - \theta_{\psi,1}(q) - \theta_{\psi,2}(q) \geq 0$, where the equality holds if and only if the q -th univariate marginals of G_1 and G_2 are identical (see, e.g., Baringhaus and Franz, 2010). So, for any fixed d , we have $\bar{\mathcal{E}}_{\psi,d} = \frac{1}{d} \sum_{q=1}^d \mathcal{E}_\psi(q) > 0$ unless G_1 and G_2 have identical univariate marginals along all coordinate axes. Therefore, it is somewhat reasonable to assume that $\liminf_{d \rightarrow \infty} \bar{\mathcal{E}}_{\psi,d} > 0$. If this assumption holds and h is concave, we can show (see the proof of Theorem 3) that $\liminf_{d \rightarrow \infty} \tilde{\delta}_{h,\psi,d} > 0$ or in other words, for $i \leq \tau < j$, $\delta_{h,\psi}(\mathbf{X}_i, \mathbf{X}_j)$ remains bounded away from zero with probability converging to one. As a result, the neighborhood structure is retained. So, if $\delta_{h,\psi}$ is used for k -means clustering, the resulting change-point detection methods $\text{RI}_{h,\psi}$ and $\text{GI}_{h,\psi}$ can perform well. This result is stated as Theorem 3.

Theorem 3. *Suppose that $\mathbf{X}_1, \dots, \mathbf{X}_\tau \stackrel{i.i.d.}{\sim} G_1$ and $\mathbf{X}_{\tau+1}, \dots, \mathbf{X}_n \stackrel{i.i.d.}{\sim} G_2$, where $1 < \tau < n-1$, and G_1 and G_2 satisfy (A2). If $\liminf_{d \rightarrow \infty} \bar{\mathcal{E}}_{\psi,d} > 0$, h is a uniformly continuous, concave function and $\binom{n}{\tau} > 2/\alpha$, then $\text{RI}_{h,\psi}$ and $\text{GI}_{h,\psi}$ with associated level α ($0 < \alpha < 1$) detect the true change-point τ with probability converging to 1 as d grows to infinity.*

There are several choices of ψ , including $\psi(t) = 1 - e^{-\sqrt{t}}$, which have non-constant completely monotone derivatives (see Baringhaus and Franz, 2010). The function $\psi(t) = t$ used in δ_0 , however, does not have this property. In addition to δ_0 , in this article, we use the dissimilarity measure $\delta_{h,\psi}$ based on $\psi(t) = 1 - e^{-\sqrt{t}}$ and $h(t) = t$ for our numerical work. The corresponding dissimilarity measure $\delta_{h,\psi}$ is referred to as δ_1 , and the resulting methods based on Rand index and Gini index are referred to as RI_1 and GI_1 , respectively. Note that the use of bounded ψ ensures finiteness of $E\left\{\psi\left((\mathbf{X}_i^{(q)} - \mathbf{X}_j^{(q)})^2\right)\right\}$ for all $q = 1, 2, \dots, d$ and $i, j = 1, 2, \dots, n$. We do not need to assume any moment condition on the underlying distributions. We have seen that in Example D, where RI_0 and GI_0 did not work well, RI_1 and GI_1 had excellent performance (see Figure 6).

From Theorem 3 and our discussion before that theorem, it is clear that RI_1 and GI_1 can perform well even when the two distributions G_1 and G_2 have the same mean and the same dispersion matrix, but they differ in their univariate marginals. We consider one such example (call it Example E) for demonstration, where the underlying 200-dimensional distributions, G_1 and G_2 , have i.i.d. coordinate variables. In G_1 they have $N(0, 2)$ distribution, but in G_2 they follow standard t_4 -distribution (t -distribution with 4 degrees of freedom). We generated the first 20 observations from G_1 and the next 20 from G_2 . This experiment was repeated 100 times as before. Figure 7 clearly shows that RI_1 and GI_1 performed well in this example. While RI_0 and GI_0 had poor performance, RI_1 and GI_1 could successfully differentiate the two distributions differing outside the first two moments.

Recall that the assumption $\liminf_{d \rightarrow \infty} \bar{\mathcal{E}}_{\psi,d} > 0$ used in Theorem 3 implies that $\liminf_{d \rightarrow \infty} \tilde{\delta}_{h,\psi,d} > 0$. However, in some cases, we can relax this condition and prove the high dimensional consistency of $\text{RI}_{h,\psi}$ and $\text{GI}_{h,\psi}$ even when the limiting value of $\tilde{\delta}_{h,\psi,d}$ is 0. Let $O(v_{\psi,d,r,s}^2)$ denote the asymp-

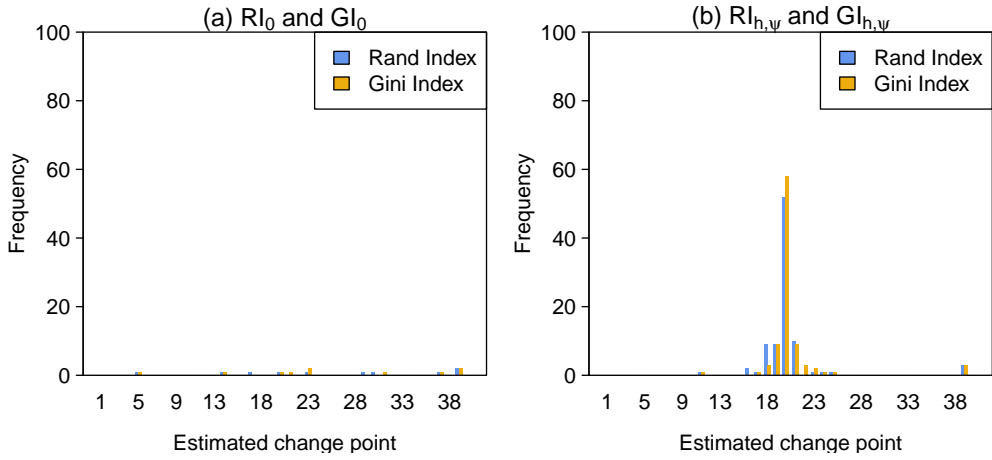


Figure 7: Frequency distribution of change-points estimated by (a) RI_0 and GI_0 and (b) $RI_{h,\psi}$ and $GI_{h,\psi}$ with $h(t) = t$ and $\psi(t) = 1 - e^{-\sqrt{t}}$ in Example E.

otic order of $Var\left(\sum_{q=1}^d \psi((X_i^{(q)} - X_j^{(q)})^2)\right)$ for $\mathbf{X}_i \sim G_r$, $\mathbf{X}_j \sim G_s$ ($r, s = 1, 2$) and $v_{\psi,d}^2 = \max\{v_{\psi,d,1,1}^2, v_{\psi,d,1,2}^2, v_{\psi,d,2,2}^2\}$. In view of (A2), one can assume that $v_{\psi,d}/d \rightarrow 0$ as d grows to infinity. The following theorem shows that if $\tilde{\delta}_{h,\psi,d}$ has higher asymptotic order than $v_{\psi,d}/d$ (i.e., $\tilde{\delta}_{h,\psi,d} d/v_{\psi,d}$ diverges to infinity as d increases), for some appropriate choices of h and ψ , $RI_{h,\psi}$ and $GI_{h,\psi}$ can successfully detect the true change-point in high dimensions. So, if the coordinate variables in G_1 and G_2 are independent or m -dependent, it is enough to have $\tilde{\delta}_{h,\psi,d}$ with asymptotic order higher than $d^{-1/2}$.

Theorem 4. *Suppose that $\mathbf{X}_1, \dots, \mathbf{X}_\tau \stackrel{i.i.d.}{\sim} G_1$ and $\mathbf{X}_{\tau+1}, \dots, \mathbf{X}_n \stackrel{i.i.d.}{\sim} G_2$, where $1 < \tau < n-1$, and G_1 and G_2 satisfy (A2). Assume that h is concave and Lipschitz continuous. If $\binom{n}{\tau} > 2/\alpha$ and $\tilde{\delta}_{h,\psi,d} d/v_{\psi,d}$ diverges to infinity as d increases, then $RI_{h,\psi}$ and $GI_{h,\psi}$ with associated level α ($0 < \alpha < 1$) detect the true change-point τ with probability converging to 1 as d grows to infinity.*

To study the high-dimensional behavior of RI_1 and GI_1 under sparse signals, we consider an example somewhat similar to Example E, where the coordinate variables are independently distributed both in

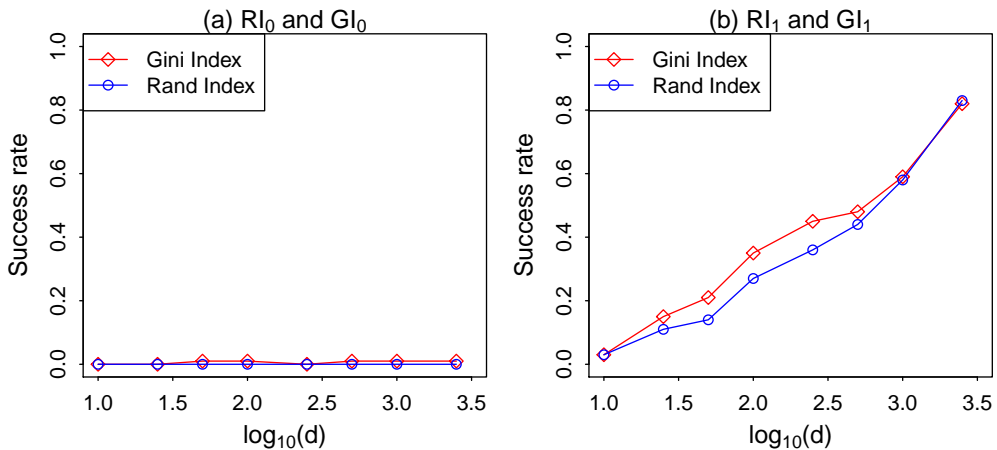


Figure 8: Success rates of (a) RI_0 and GI_0 and (b) RI_1 and GI_1 under sparse signals when some standard normal coordinate variables are replaced by standard Cauchy variables.

G_1 and G_2 . In G_1 , all d variables are i.i.d. $N(0, 1)$. The distribution G_2 differs from G_1 only in the first $d_* = \lfloor d^{2/3} \rfloor$ many coordinates, where the coordinate variables have the standard Cauchy distribution. We generated the first 20 observations from G_1 and the next 20 from G_2 , and this was repeated 100 times as before to evaluate the performance of the proposed methods. This experiment was carried out for several choices of d , and the results are reported in Figure 8. In this example, RI_0 and GI_0 had poor performance, but for RI_1 and GI_1 , the success rates gradually climbed up as d increased. Note that here G_2 does not have finite moments along all coordinates. So, (A1) does not hold, but (A2) holds for bounded ψ function. Figure 8 shows the advantage of working with a bounded ψ function in the presence of a heavy-tailed distribution.

4 Results from the analysis of simulated and benchmark data sets

In Section 3, we analyzed some simulated data sets to study the high-dimensional behavior of the proposed methods when different dissimilarity measures were used for clustering. In this section, we analyze a few more data sets to compare the performance of the proposed methods with some state-of-the-art methods. In particular, we use the E-divisive method based on averages of inter-point distances (Matteson and James, 2014), the method based on kernel (Harchaoui et al., 2008) and the graph-based methods proposed in Chen and Zhang (2015). Among the graph-based methods, we consider the ones based on minimum spanning tree (MST), nearest neighbor graph (NNG) and minimum distance pairing (MDP). As we have mentioned before, the performance of the kernel method depends heavily on the associated smoothing parameter. For each example, we considered several choices of the bandwidth and reported the best result. For our proposed methods, we used clustering based on δ_0 and δ_1 . The resulting methods are referred to as RI_0 , GI_0 , RI_1 and GI_1 , respectively. R codes for E-divisive and kernel methods are available at the R package ‘ecp’, and those for the graph-based methods can be obtained at the R package ‘gSeg’. For our proposed methods, we used our own R codes, which are available from the first author on request. Throughout this article, the level associated with the hypothesis part is taken as 0.05.

4.1 Analysis of simulated data sets

We use six simulated examples each involving 40 observations from 250-dimensional distributions. The first τ observations are generated from one distribution (call it G_1) and the rest from the other (call it G_2). We consider three different choices of τ (10, 20 and 30), and in each case, the experiment is repeated 100 times as before. The performance of different methods is summarized in Table 1.

In the first two examples, we consider two multivariate normal distributions differing in their locations and scales, respectively. But unlike the examples in Section 3, here we deal with correlated coordinate variables. In *Example 1*, two normal multivariate distributions have the same scatter matrix $\Sigma_0 =$

$((0.9^{|i-j|}))_{250 \times 250}$ but different mean vectors $\mathbf{0}_{250}$ and $\mathbf{1}_{250}$, respectively. In this location problem, barring MDP, all methods performed well. Among them, the kernel method had the best performance followed by the E-divisive method. MST had comparatively lower success rates.

		$\tau = 10$								$\tau = 20$								$\tau = 30$							
		$\hat{\tau} - \tau$	0	1	2	3	4	5	≥ 6	Total	0	1	2	3	4	5	≥ 6	Total	0	1	2	3	4	5	≥ 6
Example 1	RI ₀	73	8	4	3	2	0	5	95	74	9	8	1	0	1	1	94	73	19	4	0	0	0	1	97
	GI ₀	81	12	1	1	1	0	1	97	78	10	4	1	1	1	0	95	74	18	4	1	0	0	2	99
	RI ₁	75	10	4	3	3	1	1	97	77	10	8	0	0	4	0	99	75	14	4	1	1	0	1	96
	GI ₁	81	12	3	3	1	0	0	100	78	12	6	0	0	2	1	99	77	17	3	1	0	0	1	99
	E-divisive	90	9	0	0	0	0	1	100	86	8	3	0	0	0	3	100	84	6	1	1	0	0	8	100
	Kernel	94	6	0	0	0	0	0	100	88	9	3	0	0	0	0	100	91	8	1	0	0	0	0	100
	MST	68	10	8	1	4	1	7	99	66	18	6	2	0	1	7	100	64	11	2	6	1	1	11	96
	NNG	85	11	2	1	1	0	0	100	83	12	5	0	0	0	0	100	81	12	4	2	1	0	0	100
	MDP	44	6	6	6	0	5	30	97	51	13	5	1	2	0	22	94	37	15	5	3	3	1	26	90
Example 2	RI ₀	67	8	2	4	3	1	2	87	87	8	1	1	0	1	0	98	85	12	0	1	2	0	0	100
	GI ₀	69	10	2	4	4	0	3	92	89	8	1	1	0	0	1	100	85	13	0	1	1	0	0	100
	RI ₁	79	8	4	1	1	0	3	96	87	7	4	1	0	1	0	100	93	6	0	1	0	0	0	100
	GI ₁	79	10	3	1	3	0	3	99	88	7	3	1	0	1	0	100	93	6	0	1	0	0	0	100
	E-divisive	10	4	2	0	1	1	7	25	41	16	7	5	2	0	7	78	27	16	6	3	1	1	3	57
	Kernel	54	14	7	3	3	3	16	100	82	10	5	3	0	0	0	100	89	10	1	0	0	0	0	100
	MST	0	0	0	0	1	3	28	32	0	0	0	0	0	0	17	17	0	0	0	0	0	0	14	14
	NNG	0	0	0	0	0	0	8	8	0	0	0	0	0	0	3	3	0	0	0	0	0	0	3	3
	MDP	12	3	0	3	2	1	25	46	12	3	1	0	1	0	27	44	6	1	1	1	2	1	25	37
Example 3	RI ₀	15	7	6	4	6	6	11	55	4	3	2	3	0	2	23	37	0	1	0	0	0	0	7	8
	GI ₀	33	13	12	6	5	3	11	83	29	16	6	5	0	2	13	71	3	3	0	4	2	2	8	22
	RI ₁	42	13	10	4	9	4	8	90	44	8	11	4	12	1	14	94	16	9	12	5	4	3	17	66
	GI ₁	68	17	5	2	2	4	2	100	74	15	3	3	2	0	2	99	51	18	6	5	5	0	4	89
	E-divisive	65	13	8	3	3	2	6	100	75	15	2	2	1	0	4	99	61	18	4	4	3	1	6	97
	Kernel	61	12	4	0	0	1	0	78	51	15	4	2	1	1	1	75	19	6	3	2	3	1	5	39
	MST	0	0	0	0	0	0	13	13	0	0	0	0	0	0	18	18	0	0	0	0	0	0	22	26
	NNG	0	0	0	0	0	0	3	3	0	0	0	0	0	0	4	4	0	0	0	0	0	0	3	3
	MDP	30	10	7	0	4	10	25	86	36	6	2	1	0	2	21	68	16	7	4	3	2	1	30	63
Example 4	RI ₀	99	0	1	0	0	0	0	100	99	1	0	0	0	0	0	100	96	2	1	0	0	1	0	100
	GI ₀	100	0	0	0	0	0	0	100	99	1	0	0	0	0	0	100	97	2	0	0	0	1	0	100
	RI ₁	100	0	0	0	0	0	0	100	99	1	0	0	0	0	0	100	94	2	2	0	0	1	0	99
	GI ₁	100	0	0	0	0	0	0	100	99	1	0	0	0	0	0	100	96	2	0	0	0	1	0	99
	E-divisive	1	2	0	0	2	1	4	10	2	0	4	0	0	1	2	9	0	0	0	0	0	0	2	2
	Kernel	46	19	7	6	2	2	18	100	21	15	10	4	1	2	47	100	3	1	1	4	3	2	85	99
	MST	0	0	0	0	0	0	5	5	0	0	0	0	0	0	15	15	0	0	0	0	0	0	17	17
	NNG	0	0	0	0	0	0	6	6	0	0	0	0	0	0	4	4	0	0	0	0	0	0	3	3
	MDP	0	1	0	0	1	0	13	14	0	0	0	0	0	0	12	12	0	0	0	1	0	0	16	17
Example 5	RI ₀	0	0	0	0	0	0	2	2	1	0	0	0	1	0	2	4	1	0	0	0	0	0	2	3
	GI ₀	0	0	0	0	1	0	2	3	1	0	0	0	1	0	1	3	1	0	0	0	0	0	3	4
	RI ₁	47	4	3	0	0	0	2	56	90	0	0	0	0	0	0	90	45	11	2	0	0	0	0	58
	GI ₁	48	4	2	0	0	0	2	56	90	0	0	0	0	0	0	90	47	10	2	0	1	0	0	60
	E-divisive	0	0	0	1	0	0	8	9	1	1	0	0	0	1	9	12	0	0	0	1	0	0	2	3
	Kernel	2	7	7	6	4	3	71	100	1	5	2	6	1	3	82	100	3	6	3	2	2	8	75	99
	MST	1	2	2	3	3	0	12	23	2	2	2	1	1	0	22	30	2	4	1	3	0	1	21	32
	NNG	2	1	4	4	2	0	8	21	5	5	2	0	2	1	19	34	2	3	2	2	0	3	8	20
	MDP	4	3	0	2	1	3	26	39	3	2	1	0	1	0	25	32	5	1	1	1	2	4	21	35
Example 6	RI ₀	0	0	0	0	0	0	4	4	0	0	0	0	1	0	7	8	1	0	1	1	0	1	9	13
	GI ₀	0	0	0	0	0	0	6	6	0	0	0	0	1	0	7	8	2	0	2	0	0	1	8	13
	RI ₁	61	12	4	4	0	1	3	85	62	17	8	4	1	1	1	94	62	8	5	1	0	1	5	82
	GI ₁	63	13	3	4	0	1	3	87	58	19	11	3	2	1	0	94	63	11	4	1	0	1	4	84
	E-divisive	0	0	0	0	0	0	6	6	2	0	0	1	0	0	2	5	0	1	0	0	0	0	3	4
	Kernel	0	5	8	4	2	4	76	99	2	3	3	3	2	5	82	100	3	3	5	6	7	2	71	97
	MST	0	0	0	0	0	0	9	9	0	0	0	0	0	0	20	20	0	0	1	0	1	1	17	20
	NNG	0	0	0	0	0	0	12	12	0	0	0	0	0	0	9	9	1	1	1	0	1	0	11	15
	MDP	0	0	0	0	0	0	12	12	0	0	0	0	0	0	18	18	0	0	0	0	0	0	13	13

Table 1: Frequency distribution of $|\hat{\tau} - \tau|$ for different change-point detection methods

Example 2 deals with two multivariate normal distributions with the same mean vector $\mathbf{0}_{250}$, but different scatter matrices Σ_0 and $3\Sigma_0$, respectively, where Σ_0 is as in Example 1. In this scale problem, our proposed methods, particularly RI₁ and GI₁, outperformed their competitors. Among other methods, only the one based on kernel had somewhat competitive performance. The methods based on MST and NNG failed to detect the true change-point even on a single occasion.

In Example 3, G_2 is a symmetric distribution (standard multivariate normal), but G_1 is asymmetric. We use the multivariate geometric skew-normal distribution (see, e.g., Kundu, 2014) as G_1 . It has location parameter $\mathbf{0}_{250}$, scale parameter \mathbf{I}_{250} and skewness parameter 0.1. In this example, the E-divisive method and GI_1 had the best overall performance. The kernel method had the third best performance, but it had relatively inferior success rates for $\tau = 20$ and $\tau = 30$. Among the rest of the methods, RI_1 had better success rates, and its performance was comparable to the kernel method.

Example 4 deals with two uniform distributions. One of them is uniform on the hypercube $\{\mathbf{x} = (x_1, \dots, x_{250})^\top : |x_i| \leq 1 \forall i = 1(1)250\}$, while the other one is uniform on the hypersphere with the center at the origin and having the same volume as the hypercube mentioned above. In this example, all proposed methods had excellent performance. They detected the true change-point on almost all occasions. All graph-based methods and the E-divisive method performed poorly. The kernel method also failed to yield satisfactory results.

Example 5 and Example 6 are 250-dimensional versions of Example D and Example E (described in Section 3), respectively. Recall that in these examples, two distributions have the same location and the same trace of the dispersion matrices, while they differ in their marginals. In such cases, RI_0 and GI_0 could not differentiate between the two distributions, but RI_1 and GI_1 performed well. All other competing methods had poor performance. Note that these competing methods are based on pairwise Euclidean distances. So, when the distributions differ outside the first two moments, such a poor performance by these methods is quite expected.

Table 1 clearly shows that the proposed methods based on Gini index performed better than the corresponding methods based on Rand index in almost all examples. We also observed the same in almost all previous examples (see Figures 5-8). Therefore, in the remaining part of the article, we shall report the results for the methods based on Gini index only.

4.2 Analysis of benchmark data sets

We analyze two benchmark data sets, the Reality Mining data (see Eagle and Pentland, 2006) and the Synthetic Control Chart data (see Alcock and Manolopoulos, 1999), for further comparison. The Reality Mining data set is available at MIT Media Laboratory Website (<http://realitycommons.media.mit.edu/realitymining.html>). The Synthetic Control Chart data set can be obtained from the UCI Machine Learning Repository (<https://archive.ics.uci.edu>).

Reality Mining data were collected when the MIT Media Laboratory conducted a study on several individuals including the university students and staffs, using mobile phones with pre-installed software recording call logs from July 20, 2004 to June 14, 2005. The data set contains information on the caller, the callee and the time for every call that was made during this period. Here the question of interest is whether there is any change in the phone call pattern during this time. This data set contains some missing values. We delete those observations with missing values and deal with the information on 84

individuals. From this data set, we construct a 84×84 matrix for each of the 48 weeks, where the (i, j) entry of the matrix is taken as 1 when there is at least one attempt for communication between the i -th and the j -th individuals in that week. We consider the $\binom{84}{2} = 3486$ distinct elements of the adjacency matrix as elements of a 3486-dimensional vector to carry out our analysis.

The proposed methods, GI_0 and GI_1 , detected week 22 (Dec 14-20, 2004) as the change-point (see Figure 9). Note that this week was the beginning of the winter break when the students and staffs were moving from fall session to spring session. This provides a justification for the selection of this week as a change-point in friendship network pattern. Among the other methods, E-divisive selected week 7 (Aug 31-Sep 06, 2004) and the kernel method selected week 36 (Mar 22-28, 2005) as the change-point. The graph-based methods, MST, NNG and MDP, detected the change-point at week 41 (Apr 26-May 02, 2005), week 33 (Feb 28-Mar 07, 2005) and week 4 (Aug 10-16, 2004), respectively.

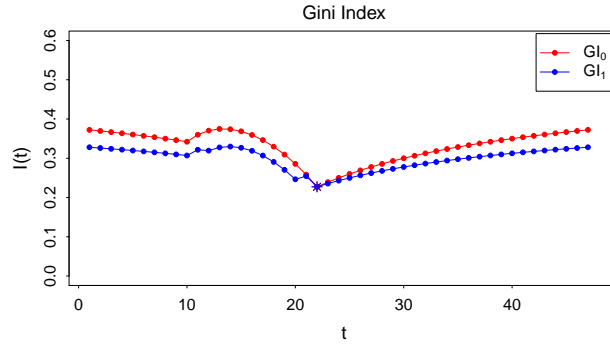


Figure 9: Gini index for different choices of t in Reality Mining data set.

Synthetic Control Chart Data set contains 600 examples of control charts synthetically generated by the process in Alcock and Manolopoulos (1999). There are six different classes of control charts each containing 100 examples, where each example is represented by an observation on a 60-dimensional vector. For our experiment, we consider the observations from two classes: ‘Normal’ and ‘Cyclic’. While the observations in the ‘Normal’ class are like white noises, those in the ‘Cyclic’ class show cyclic patterns. Some observations from ‘Normal’ and ‘Cyclic’ classes are shown in Figure 10.

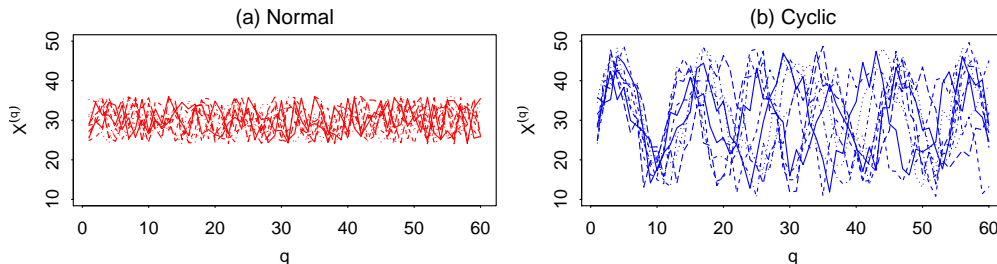


Figure 10: Examples of ‘Normal’ and ‘Cyclic’ patterns in Synthetic Control Chart data.

In this example, first we carried out an experiment with the full data set consisting of 200 observations, where the observations from the ‘Normal’ (respectively, ‘Cyclic’) class were used as the first

(respectively, last) 100 observations. So, there was a change-point at 100. All competing methods considered in this article successfully detected the change-point. Based on that single experiment, it was not possible to compare among different methods. So, next we performed our experiment using only 10 observations from each class. We chose the first 10 observations randomly from the set of 100 ‘Normal’ patterns and the next 10 from the set of ‘Cyclic’ patterns. Different methods were used on this data set to check whether they can successfully detect the change-point at 10. We repeated this experiment 100 times, and the results are reported in Figure 11. In this example, our proposed methods, particularly GI_1 , outperformed their all competitors. The E-divisive method had the third best performance. Graph-based methods, MST and NNG, had relatively lower success in detecting the true change-point. The performance of the kernel method was even worse. In this example, we could not report the performance of MDP as the corresponding R codes returned some errors.

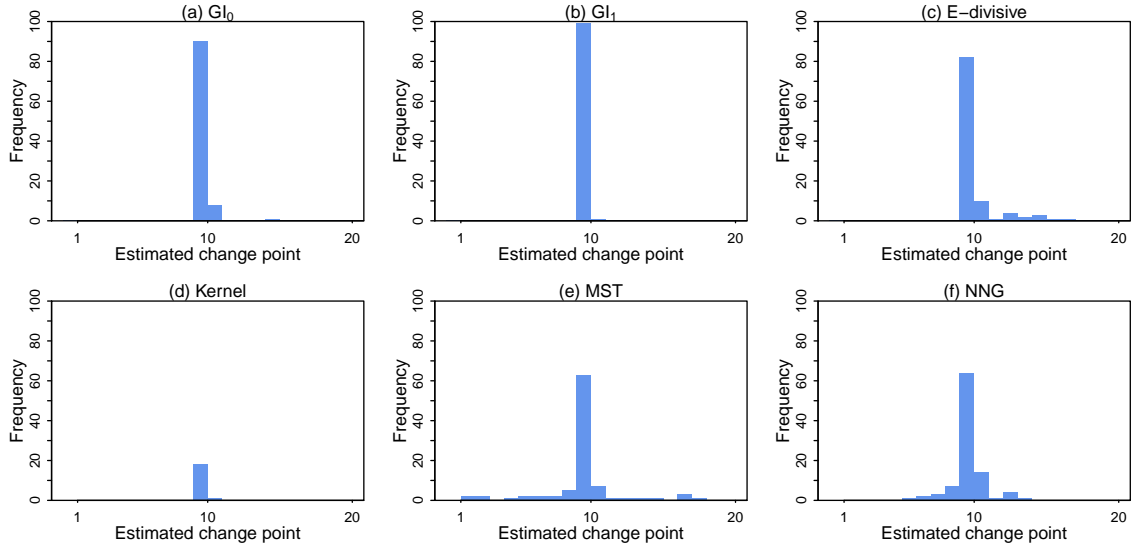


Figure 11: Frequency distribution of change-points estimated by different methods in Synthetic Control Chart data set.

5 Multiple change-point detection

So far, we have assumed that there is at most one change-point in a sequence of observations. However, in practice, we may have changes in more than one location. To take care of this problem, in this section, we modify our algorithms for multiple change-points detection. At first, our algorithms aim at finding the most notable change in the sequence $\mathbf{X}_1, \mathbf{X}_2, \dots, \mathbf{X}_n$ and then test for the statistical significance of that change. If the change is found to be statistically insignificant, the algorithm stops by suggesting no existence of change-points in the data. If it is found to be statistically significant, the location corresponding to that change (say, t) is considered as the change-point. In that case, we use the algorithm again on the left sub-sequence $\mathbf{X}_1, \mathbf{X}_2, \dots, \mathbf{X}_t$ and right sub-sequence $\mathbf{X}_{t+1}, \mathbf{X}_{t+2}, \dots, \mathbf{X}_n$ separately to find other possible change-points in the data.

To find the most notable change-points in $\mathbf{X}_1, \mathbf{X}_2, \dots, \mathbf{X}_n$, first we use k -means clustering (with $k = 2$) based on δ_0 or $\delta_{h,\psi}$ on this data set. This leads to a sequence of red and blue dots as before. Now, for any (t, s) with $1 \leq t < s \leq n$, we check how different the two subsequences $\mathbf{X}_1, \mathbf{X}_2, \dots, \mathbf{X}_t$ and $\mathbf{X}_{t+1}, \mathbf{X}_{t+2}, \dots, \mathbf{X}_s$ are. For this purpose, we compute the impurity $\mathcal{I}_{t,s}$ given by

$$\mathcal{I}_{t,s} = \frac{t}{s} \Phi(p_{1,t}) + \frac{s-t}{s} \Phi(p_{t+1,s}),$$

where $p_{1,t}$ and $p_{t+1,s}$ are the proportions of red dots in the two subsequences, and Φ is an impurity function as discussed in Section 2. Here also, we use Gini index $\Phi(p) = 2p(1-p)$ as the impurity function. We compute $\mathcal{I}_{t,s}$ for different choices of t and s . Note that these impurities are computed based on sequences of different lengths. So, unlike before, they are not comparable. Therefore, instead of the $\mathcal{I}_{t,s}$'s, we look at their corresponding p -values. Recall that given the numbers of red and blue dots (i.e., the numbers of observations in the first and the second clusters) in the sequence of length s , $\mathcal{I}_{t,s}$ has the distribution-free property under \mathcal{H}_0 (see Section 2). So, the corresponding p -value $p_{t,s}$ can be computed easily. Note that these p -values do not depend on the choice of the impurity function $\Phi(p)$ as long as it is a monotone function of $|p - \frac{1}{2}|$. Let (t_0, s_0) be the value of (t, s) for which $p_{t,s}$ is minimum. We consider t_0 as the most potential change-point and use $p_{\min} = p_{t_0, s_0}$ as the test statistic to test for its statistical significance. We reject \mathcal{H}_0 at level α if p_{\min} is smaller than the corresponding threshold, and in that case, t_0 is selected as the change-point. One can use the permutation method to determine the cut-off. However, note that just like R_{\min} or \mathcal{I}_{\min} (see Section 2), p_{\min} is also a function of the arrangement of all red and blue dots. So, it also has the distribution-free property, and hence it is possible to compute the cut-off offline. Instead of impurity function, one can use Rand index as well. But our empirical experience suggests that the methods based on impurity function (Gini index) usually perform better than those based on Rand index.

We analyze some simulated data sets to evaluate the performance of the proposed methods. We use clustering based on δ_0 or δ_1 as before, and the corresponding methods based on Gini index are referred to as GI_0 and GI_1 , respectively. We also report the performance of E-divisive and kernel methods. Since the graph-based methods, MST, NNG and MDP, are not applicable to multiple change-point problems (except for some special cases, where observations from two distributions appear repeatedly), we could not use them for comparison. In this section, we consider 4 examples (Examples 7-10). In each of these examples, we deal with 250-dimensional distributions and generate sequences of 60 observations containing 2 or 3 change-points. Each experiment is repeated 100 times as before to assess the performance of different methods. The kernel method needs the maximum number of change-points to be mentioned by the user. Here, we use the actual number of change-points for this purpose. The E-divisive method needs the minimum gap between two change-points to be specified. For this method and our proposed methods, we maintain a minimum gap of 5.

In Example 7, we have observations from two Gaussian distributions differing only in their means. Observations 1 to 15 and 31 to 45 are generated from $N_{250}(0.5\mathbf{1}_{250}, \mathbf{I}_{250})$ and the rest from $N_{250}(\mathbf{0}_{250}, \mathbf{I}_{250})$.

So, there are 3 change-points at 15, 30 and 45. In this location problem, GI_0 and GI_1 performed well, but E-divisive and Kernel methods outperformed them (see Figure 12). However, we observed a completely different picture in *Example 8*, which deals with four Gaussian distributions $N_{250}(\mathbf{0}_{250}, (\frac{1}{20})^{i-1} \mathbf{I}_{250})$ ($i = 1, 2, 3, 4$) differing only their scales. The first 15 observations are generated from the first distribution $N_{250}(\mathbf{0}_{250}, \mathbf{I}_{250})$, the next 15 from the second, and so on. In this example, GI_0 and GI_1 outperformed the other two methods. Among the proposed methods, GI_0 performed slightly better. On almost all occasions, E-divisive and kernel methods failed to detect the change-point at 45.

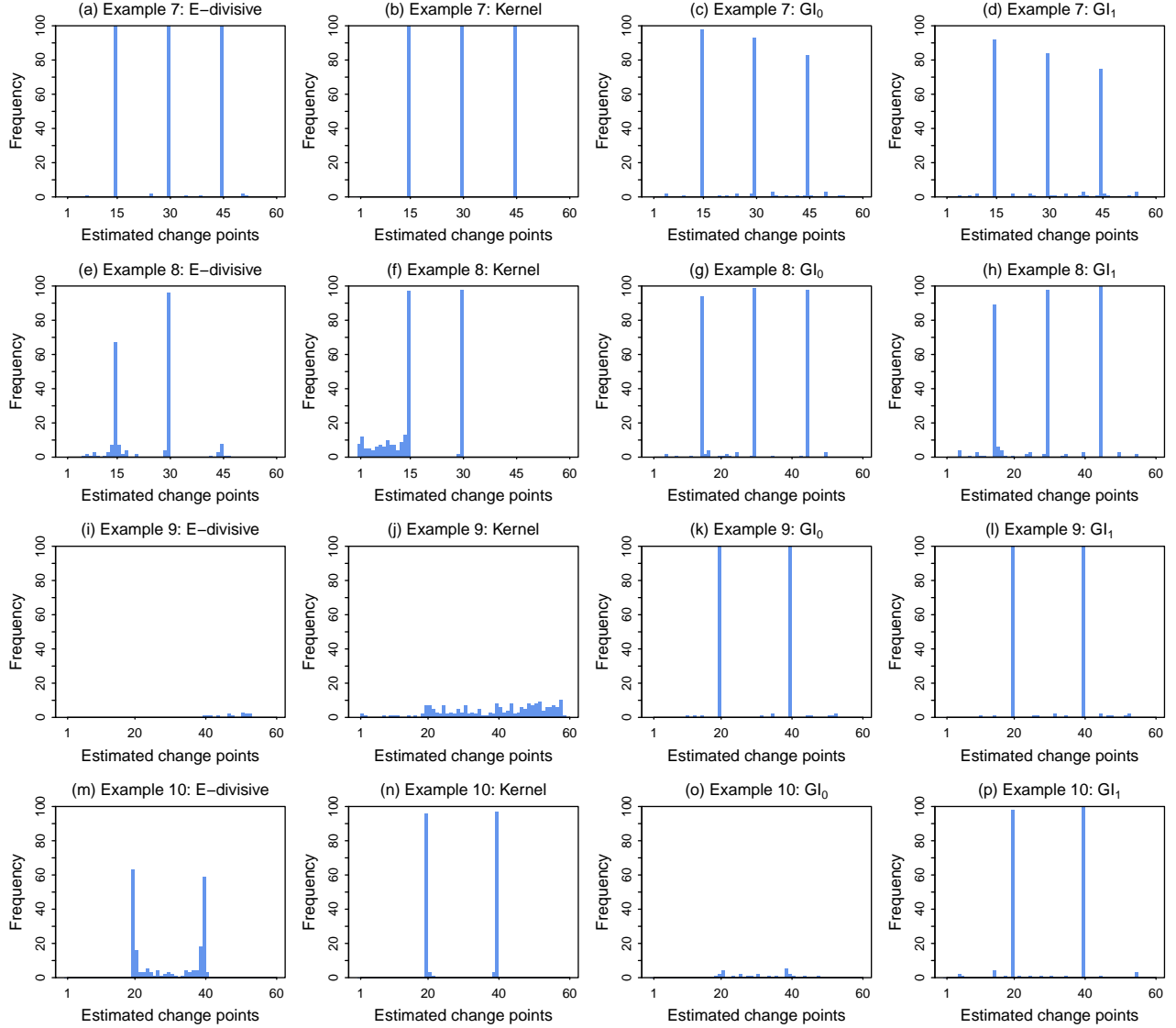


Figure 12: Frequency distribution of change-points estimated by different methods in Examples 7-10.

In *Example 9*, observations are generated from three distributions (G_1 , G_2 and G_3 , say) differing only in their first 50 coordinates. The first 50 coordinate variables in G_i ($i = 1, 2, 3$) jointly follow the uniform distribution on the region $\{\mathbf{x} \in \mathbb{R}^{50} : 2(i-1) \leq \|\mathbf{x}\| \leq 2i-1\}$. 200 variables generated from the uniform distribution on $\{\mathbf{x} \in \mathbb{R}^{200} : 0 \leq \|\mathbf{x}\| \leq 5\}$ are augmented with them to make the dimension

of the data 250. The first 20 observations are generated from G_1 , the next 20 from G_2 and last 20 from G_3 . Figure 12 clearly shows that in this example, while E-divisive and kernel methods performed poorly, the proposed methods had excellent performance.

Example 10 deals with observations from three distributions G_1, G_2 and G_3 , each having i.i.d. coordinate variables. The coordinate variables in G_1 follow $N(0, 2)$ distribution. In G_2 and G_3 , they follow standard Cauchy and standard Laplace distributions, respectively. Here also, the first 20 observations are generated from G_1 , the next 20 from G_2 and last 20 from G_3 . We have seen that in the presence of heavy-tailed distributions, GI_0 may not yield satisfactory results (see Figure 7). Here also we observed the same. But GI_1 performed well in this example. The kernel method also had competitive performance, but the performance of the E-divisive method was relatively poor.

We also analyze the *Lymphoma data set* available at the *R* package *spls*. It contains expression levels of 4026 genes for 42 diffuse large B-cell lymphoma (DLBCL), 9 follicular lymphoma (FL) and 11 chronic lymphocytic lymphoma (CLL). Figure 13 shows the observations from 3 classes.

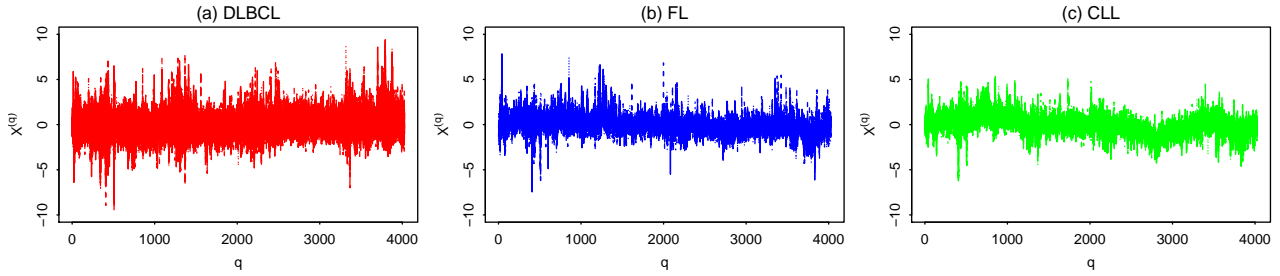


Figure 13: Observations from DLBCL, FL and CLL classes.

When we used different methods on the full data set consisting of 62 observations, the two change-points, one at 42 (transition from DLBCL to FL) and the other at 51 (transition from FL to CLL), were successfully detected by all of them. To have a meaningful comparison among these methods, next we carried out our experiment with 32 randomly chosen observations (16 from DLBCL and 8 each from FL and CLL). This experiment was repeated 100 times as before, and the results are reported in Figure 14. In this experiment, the E-divisive method and the proposed methods worked well, but the kernel method failed to discriminate between the observations coming from FL and CLL classes.

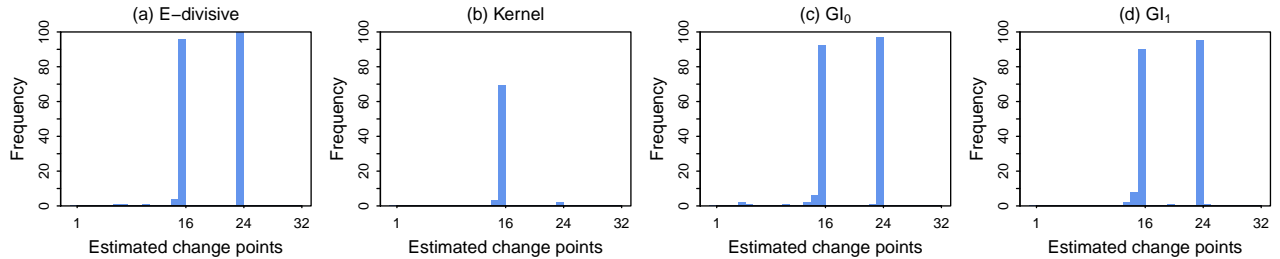


Figure 14: Frequency distribution of change-points estimated by GI_0 , GI_1 , E-divisive and kernel methods in Lymphoma data set.

6 More on change-point detection

In this section, we address some further issues related to our change-point methods. From our discussions and numerical results in previous sections, it is clear that our proposed methods can successfully detect the change-point when the two distributions differ in their locations, scales or one dimensional marginals. Now one may be curious to know whether they can differentiate two distributions differing only in their higher order marginals, e.g., when the two distributions have the same one dimensional marginals but different correlation structures. One may also like to see how these proposed methods perform when there are outliers in the data. We briefly address these issues in the following subsections.

6.1 What happens if two distributions differ in their higher order marginals?

Let us consider two examples (call them Examples 11 and 12), where the two distributions have same univariate marginals but different dispersion matrices. *In Example 11, we generate the first 80 observations from $N_{250}(\mathbf{0}_{250}, \mathbf{I}_{250})$ and the next 80 from $N_{250}(\mathbf{0}_{250}, \mathbf{\Sigma})$ with $\mathbf{\Sigma} = ((0.9^{|i-j|}))_{250 \times 250}$. In Example 12, we consider two multivariate normal distributions having block diagonal covariance matrices with each block of size 2. The blocks in the first (respectively, second) population have the diagonal elements 1 and the off-diagonal elements 0.9 (respectively, -0.9). Here also, we have first 80 observations from the first population, and the next 80 from the second. Each experiment is repeated 100 times. Figure 15 (see the figures in the left column) shows that GI_1 did not have satisfactory performance in these examples. In Example 12, it could not detect the true change-point even on a single occasion.*

We can take care of this problem if we use a block version of the dissimilarity measure. We make a partition of the observation vector $\mathbf{x} = (x^{(1)}, x^{(2)}, \dots, x^{(d)})^\top$ into b blocks $\tilde{\mathbf{x}}^{(1)}, \tilde{\mathbf{x}}^{(2)}, \dots, \tilde{\mathbf{x}}^{(b)}$, where the i -th block contains d_i variables ($\sum_{i=1}^b d_i = d$). The block version of the dissimilarity measure $\rho_{h,\psi}$ between two observations \mathbf{x} and \mathbf{y} is given by

$$\rho_{h,\psi}^{B\ell}(\mathbf{x}, \mathbf{y}) = h \left(\frac{1}{b} \sum_{i=1}^b \psi \left(\|\tilde{\mathbf{x}}^{(i)} - \tilde{\mathbf{y}}^{(i)}\|^2 \right) \right).$$

Using this dissimilarity measure we can construct $\delta_{h,\psi}^{B\ell}$, a block version of $\delta_{h,\psi}$. Note that if $b = d$ and $d_i = 1$ for all i , we have $\rho_{h,\psi}^{B\ell} = \rho_{h,\psi}$ and $\delta_{h,\psi}^{B\ell} = \delta_{h,\psi}$. From our discussion in Section 3.2, it is quite clear that if we use $\delta_{h,\psi}^{B\ell}$ for k -means clustering, for suitable choices of h and ψ (as discussed before), the resulting change-point methods based on Rand index or Gini index can discriminate between two distributions unless their marginal block distributions (joint distribution of the random variables in a block) are identical. In fact, as long as the block sizes are bounded (which implies b grows to infinity as d increases), results similar to Theorem 3 and 4, with univariate marginals replaced by marginal block distributions, can be proved under similar assumptions. So, if we use blocks of size 2, we can discriminate between two distributions differing in their correlation structures.

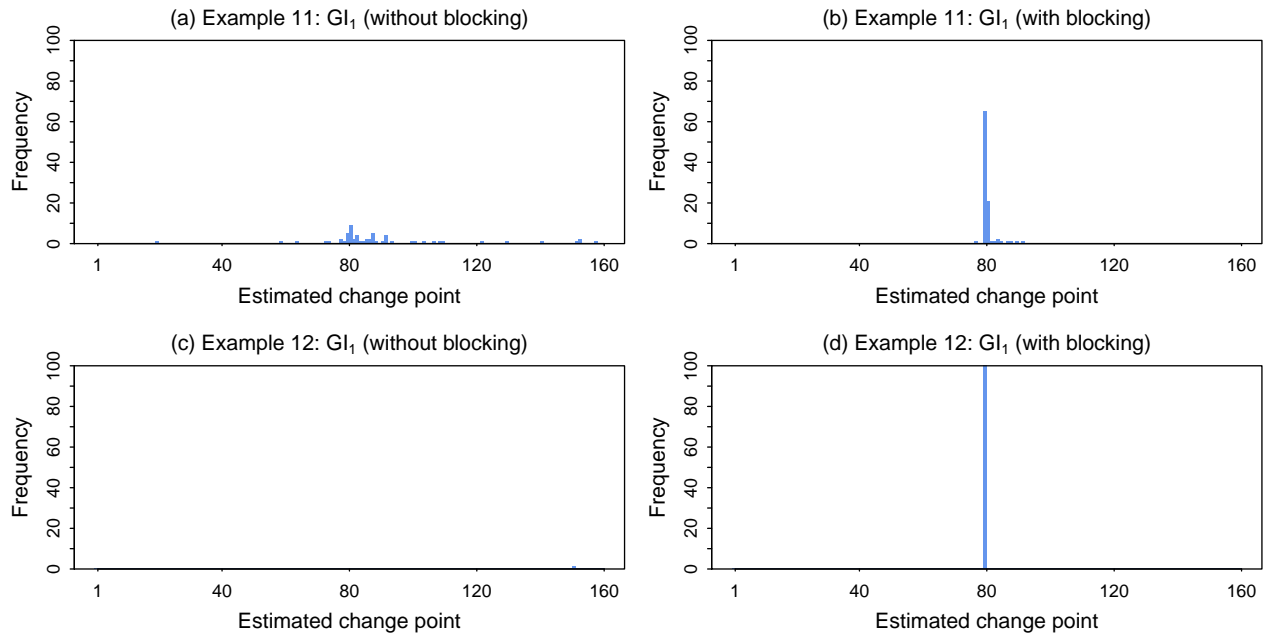


Figure 15: Frequency distribution of change-points estimated by GI_1 and its block version in Examples 11 and 12.

We observed the same in Examples 11 and 12, when we used 125 blocks each of size 2. From the description of Example 12, it is clear that here each block should be formed by taking two consecutive variables $(X^{(2i-1)}, X^{(2i)})$ for some $i = 1, 2, \dots, 125$. However, in our case, we used a data-driven method for the formation of blocks. Since we want to extract more information from the joint distribution of the variables, ideally one should form the blocks such that the variables within a block are more dependent compared to variables belonging to different blocks. So, first we measure the dependence between each pair of variables and then form the blocks such that sum of the dependence between the two variables in a block is maximum. The algorithm based on optimal non-bipartite matching (see Lu et al., 2011) is used for this maximization. Here we use the statistic based on distance correlation (see, e.g., Székely et al., 2007) to measure dependence between the variables, but one can use other appropriate measures (see, e.g., Roy et al., 2020, and the references therein) as well. When we used block version of the dissimilarity measure, our methods performed well (see the right column in Figure 15). While in Example 11, it selected the true change-point in more than 60% cases, in Example 12, the true change-point was correctly detected on all occasions.

6.2 Change-point detection in the presence of outliers

To demonstrate the effect of outliers on our methods, we reconsider the example with two univariate normal distributions $N(0, 1)$ and $N(4, 1)$ discussed in Section 1, but here we replace 4 out of 40 observations by outliers generated from the $N(25, 1)$ distribution. A scatter plot of this data set is

given in Figure 16(a). When we used clustering based on δ_0 , it put all outliers (indicated using blue dots in Figure 16(b)) in one cluster and the rest of the observations (indicated using red dots) in other. As a consequence, the true change-point could not be detected properly. But, if we look at the sequence of red and blue dots, we can observe some points (of blue color) which were preceded and followed by points of the opposite (red) color. Naturally they can be considered as anomalies and be removed from the data set. Figure 16(c) shows the scatter plot of the data set after removing those observations. When we used the same clustering method on this new data set, it led to two clusters, one consisting of observations from $N(0, 1)$ and the other consisting of observations from $N(4, 1)$ (see Figure 16(d)). As a result, the change-point was correctly detected. Now, in practice, it may not always be possible to remove out all outliers in a single round of screening. One may need to repeat this procedure several times (as long as we get observations preceded and followed by observations of opposite color) to filter out all potential outliers and work with the filtered data set. We observed the same phenomenon when clustering algorithms based on δ_1 were used.

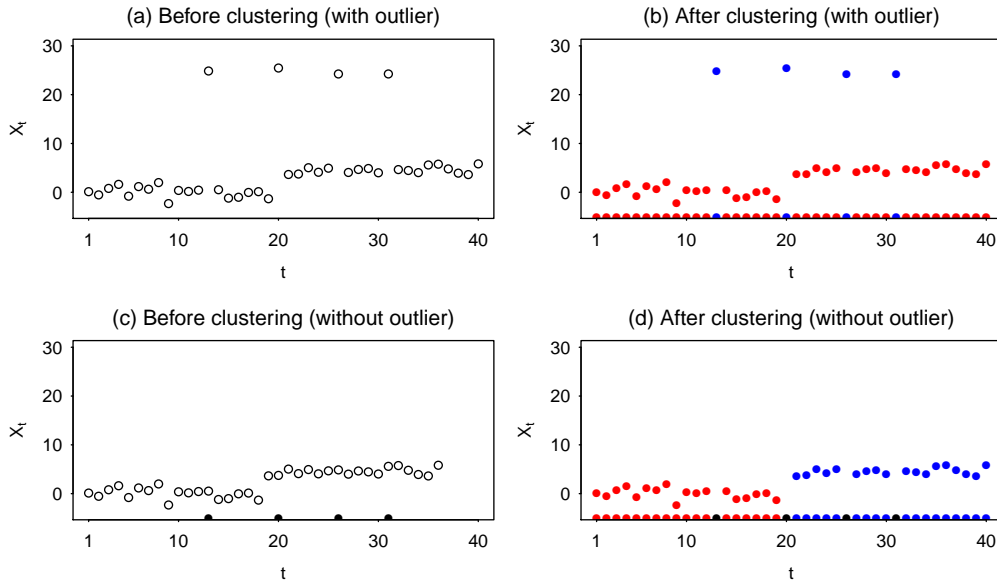


Figure 16: Clustering before and after the deletion of potential outliers.

7 Concluding remarks

In this article, we have proposed some clustering based methods for change-point detection, which can be conveniently used for high-dimensional data even when the dimension is much larger than the sample size. Under appropriate regularity conditions, we have established the high-dimensional consistency of these methods and amply demonstrated their superiority over some state-of-the-arts methods by analyzing several simulated and real data sets. From the description of our methods, it is quite clear that these methods can also be used for functional data or observations taking values in infinite dimensional Banach spaces. However, one needs to investigate theoretical and empirical

performance of these methods for such data sets. Throughout this article, though we have used k -means algorithms based on different dissimilarity measures, other clustering algorithms (e.g., k -medoids algorithms, spectral clustering, hierarchical clustering based on different types of linkages) can also be used, and for most of them, theoretical results similar to Theorems 1-4 can be derived. Similarly, one can use methods based on other appropriate dissimilarity measures. For instance, if the coordinate variables are not of comparable units and scales, it is better to standardize them before using the change-point methods. If some of the coordinate variables are categorical or ordinal, one may need to use a different type of distance functions (see, e.g., Friedman et al., 2001) for clustering. We have seen that the block version of our algorithms can successfully detect the change-points even when the underlying distributions differ only in their higher order marginals. In this article, we have used blocks of size 2 to discriminate between two distributions differing in their correlation structures. However, in practice, one may need to use blocks of different sizes. At this moment, we do not have rigorous idea about the optimum number of blocks and the block sizes to be used. This is still an open issue to be resolved. One also needs to develop a suitable algorithm for finding the optimum block configurations. In this article, we have studied some theoretical properties of the proposed methods in high dimensional asymptotic regime, where the dimension grows to infinity while the sample size remains fixed. Now, an interesting question that arises in this context is: “how will these methods perform if the sample also grows with the dimension?” Intuitively, a statistical method is expected to perform better if we have more observations. But one needs to carry out theoretical investigations in this regard.

Appendix

Proof of Lemma 1: Suppose that the clustering algorithm puts t_{0i} out of first t_0 observations, and n_i out of total n observations in the i -th ($i = 1, 2$) cluster ($t_{01} + t_{02} = t_0$, $n_1 + n_2 = n$). Without loss of generality, also assume that it assigns \mathbf{x}_{t_0} and \mathbf{x}_{t_0+1} to the first cluster. So, the Rand index at t_0 is

$$\begin{aligned} R(t_0) &= \binom{n}{2}^{-1} \{t_{01}t_{02} + (n_1 - t_{01})(n_2 - t_{02}) + t_{01}(n_1 - t_{01}) + t_{02}(n_2 - t_{02})\} \\ &= \binom{n}{2}^{-1} (n_1 - t_{01} + t_{02})(n_2 - t_{02} + t_{01}). \end{aligned}$$

Therefore, $\binom{n}{2}R(t_0) = \beta_1\beta_2$, where $\beta_1 = n_1 - t_{01} + t_{02}$ and $\beta_2 = n_2 - t_{02} + t_{01}$. Now out of the first $t_0 - 1$ (respectively, $t_0 + 1$) observations, $t_{01} - 1$ (respectively, $t_{01} + 1$) are assigned to the first cluster, and t_{02} observations to the second cluster. So, replacing t_{01} by $t_{01} - 1$ (respectively, $t_{01} + 1$), we get $\binom{n}{2}R(t_0 - 1) = (\beta_1 + 1)(\beta_2 - 1)$ and $\binom{n}{2}R(t_0 + 1) = (\beta_1 - 1)(\beta_2 + 1)$. Therefore,

$$\binom{n}{2} \{2R(t_0) - R(t_0 - 1) - R(t_0 + 1)\} = 2.$$

This implies $R(t_0) > \min\{R(t_0 - 1), R(t_0 + 1)\}$. So, $R(t)$ cannot be minimized at $t = t_0$. \square

Proof of Lemma 2: Suppose that the clustering algorithm assigns n_i out of n observations to the i -th ($i = 1, 2$) cluster ($n_1 + n_2 = n$). Without loss of generality, assume that it puts \mathbf{x}_{t_0} and \mathbf{x}_{t_0+1} to the first cluster. Also assume that t_{0i} out of first t_0 observations are assigned to the i -th ($i = 1, 2$) cluster, where $t_{01} + t_{02} = t_0$. So, the impurity function at t_0 is given by

$$\mathcal{I}(t_0) = \frac{t_0}{n} \Phi\left(\frac{t_{01}}{t_0}\right) + \frac{n-t_0}{n} \Phi\left(\frac{n_1-t_{01}}{n-t_0}\right) = A_{t_0} + B_{t_0}, \text{ say.}$$

Note that out of the first $t_0 - 1$ (respectively, $t_0 + 1$) observations, there are $t_{01} - 1$ (respectively, $t_{01} + 1$) observations from the first cluster. So,

$$\mathcal{I}(t_0 - 1) = \frac{t_0 - 1}{n} \Phi\left(\frac{t_{01} - 1}{t_0 - 1}\right) + \frac{n - t_0 + 1}{n} \Phi\left(\frac{n_1 - t_{01} + 1}{n - t_0 + 1}\right) = A_{t_0-1} + B_{t_0-1},$$

$$\mathcal{I}(t_0 + 1) = \frac{t_0 + 1}{n} \Phi\left(\frac{t_{01} + 1}{t_0 + 1}\right) + \frac{n - t_0 - 1}{n} \Phi\left(\frac{n_1 - t_{01} - 1}{n - t_0 - 1}\right) = A_{t_0+1} + B_{t_0+1}.$$

Since $\frac{t_{01}}{t_0} = \frac{t_0-1}{2t_0} \left(\frac{t_{01}-1}{t_0-1}\right) + \frac{t_0+1}{2t_0} \left(\frac{t_{01}+1}{t_0+1}\right)$, using strict concavity of Φ , we have

$$\Phi\left(\frac{t_{01}}{t_0}\right) > \frac{t_0-1}{2t_0} \Phi\left(\frac{t_{01}-1}{t_0-1}\right) + \frac{t_0+1}{2t_0} \Phi\left(\frac{t_{01}+1}{t_0+1}\right).$$

Multiplying both sides by t_0/n , we get $A_{t_0} > \frac{1}{2}(A_{t_0-1} + A_{t_0+1})$. Similarly, we can show that $B_{t_0} > \frac{1}{2}(B_{t_0-1} + B_{t_0+1})$. Combining these two, one obtains $\mathcal{I}(t_0) > \frac{1}{2}(\mathcal{I}(t_0-1) + \mathcal{I}(t_0+1))$. This implies $\mathcal{I}(t_0) > \min\{\mathcal{I}(t_0-1), \mathcal{I}(t_0+1)\}$. So, $\mathcal{I}(t)$ cannot be minimized at $t = t_0$. \square

Lemma 3. Suppose that $\mathbf{X}_1(d), \dots, \mathbf{X}_n(d)$ are d -dimensional random vectors such that as $d \rightarrow \infty$,

- (a) $d^{-1} \|\mathbf{X}_i(d) - \mathbf{X}_j(d)\|^2 \xrightarrow{P} \theta_1$ for $i < j \leq \tau$,
- (b) $d^{-1} \|\mathbf{X}_i(d) - \mathbf{X}_j(d)\|^2 \xrightarrow{P} \theta_2$ for $\tau < i < j$ and
- (c) $d^{-1} \|\mathbf{X}_i(d) - \mathbf{X}_j(d)\|^2 \xrightarrow{P} \theta_3$ for $i \leq \tau < j$.

For any non-empty proper subset S of $S_n = \{1, 2, \dots, n\}$, define $\lambda_0(S) = \frac{1}{2|S|} \sum_{i, i' \in S} \|\mathbf{X}_i(d) - \mathbf{X}_{i'}(d)\|^2 + \frac{1}{2|S^c|} \sum_{j, j' \in S^c} \|\mathbf{X}_j(d) - \mathbf{X}_{j'}(d)\|^2$ (note that $\lambda_0(S) = \lambda_0(S^c)$ for all S). Let S_0 be a minimizer of $\lambda_0(S)$. Now, as d tends to infinity, we have the following results.

- (i) If $\theta_3 > \max\{\theta_1, \theta_2\}$, then $P((S_0 = S_\tau) \cup (S_0 = S_\tau^c)) \rightarrow 1$, where $S_\tau = \{1, 2, \dots, \tau\}$ and $S_\tau^c = S \setminus S_\tau$.
- (ii) If $\theta_1 < \theta_2$ and $\theta_3 = (\theta_1 + \theta_2)/2$, then $P(|S_0| = 1 \text{ or } |S_0^c| = 1) \rightarrow 1$, where this singleton set contains some $j > \tau$.

Proof: (i) Note that as $d \rightarrow \infty$, $\lambda_0(S_\tau)/d = \lambda_0(S_\tau^c)/d \xrightarrow{P} \frac{1}{2}[(\tau-1)\theta_1 + (n-\tau-1)\theta_2] = \beta_0$, say. Now, consider a subset S of S_n , with $|S| = k$, $\sum_{i=1}^\tau \mathbb{I}\{i \in S\} = k_1$ and $\sum_{i=\tau+1}^n \mathbb{I}\{i \in S\} = k_2$ ($k_1 + k_2 = k$).

Let us first consider the case, where either $k_1 = 0$ or $k_2 = 0$. When $k_2 = 0$ (i.e., $k_1 = k$), from the definition, it is clear that $S \subseteq S_\tau$ and hence $k \leq \tau$. However, if $k = \tau$, S matches with S_τ . So, let us

assume $k < \tau$. For such a subset S , we have

$$\begin{aligned} \frac{\lambda_0(S)}{d} &\xrightarrow{P} \frac{(k-1)\theta_1}{2} + \frac{1}{2(n-k)} [(\tau-k)(\tau-k-1)\theta_1 + (n-\tau)(n-\tau-1)\theta_2 + 2(\tau-k)(n-\tau)\theta_3] \\ &= \frac{(k-1)\theta_1}{2} + \frac{1}{2} [a_1(\tau-k-1)\theta_1 + a_2(n-\tau-1)\theta_2 + a_1(n-\tau)\theta_3 + a_2(\tau-k)\theta_3] = A_0, \text{ say,} \end{aligned}$$

where $a_1 = (\tau-k)/(n-k)$ and $a_2 = (n-\tau)/(n-k)$. Since $k < \tau < n$ and $\theta_3 > \max\{\theta_1, \theta_2\}$, we have $0 < a_1, a_2 < a_1 + a_2 = 1$, $a_1(n-\tau)\theta_3 \geq a_1(n-\tau-1)\theta_2 + a_1\theta_3$ and $a_2(\tau-k)\theta_3 \geq a_2(\tau-k-1)\theta_1 + a_2\theta_3$. Hence, we get $A_0 \geq \frac{1}{2}[(k-1)\theta_1] + \frac{1}{2}[(\tau-k-1)\theta_1 + (n-\tau-1)\theta_2 + \theta_3] = \beta_0 + \frac{1}{2}(\theta_3 - \theta_1) > \beta_0$.

So, $(\lambda_0(S) - \lambda_0(S_\tau))/d \xrightarrow{P} A_0 - \beta_0 > 0$ or in other words, $P(\lambda_0(S) > \lambda_0(S_\tau)) \rightarrow 1$ as $d \rightarrow \infty$. Similarly, for $k_1 = 0$ (i.e., $k_2 = k$), we have $S \subseteq S_\tau^c$ and hence $k \leq n - \tau$. Now, for $k = n - \tau$, S matches with S_τ^c and for $k < n - \tau$, we can show that $P(\lambda_0(S) > \lambda_0(S_\tau)) \rightarrow 1$ as d tends to infinity.

Also note that if $\tau - k_1 = 0$, S^c is a subset of S_τ^c , and a similar argument leads to $P(\lambda_0(S) > \lambda_0(S_\tau)) = P(\lambda_0(S^c) > \lambda_0(S_\tau^c)) \rightarrow 1$ as $d \rightarrow \infty$. Similar argument works for the case $n - \tau - k_2 = 0$ as well.

Now, consider the cases, where $k_1, k_2, \tau - k_1$ and $n - \tau - k_2$ are all positive. For such a subset S ,

$$\begin{aligned} \frac{\lambda_0(S)}{d} &\xrightarrow{P} \frac{1}{2k} [k_1(k_1-1)\theta_1 + k_2(k_2-1)\theta_2 + 2k_1k_2\theta_3] + \frac{1}{2(n-k)} [(\tau-k_1)(\tau-k_1-1)\theta_1 \\ &\quad + (n-\tau-k_2)(n-\tau-k_2-1)\theta_2 + 2(\tau-k_1)(n-\tau-k_2)\theta_3] \\ &= \frac{1}{2} [b_1(k_1-1)\theta_1 + b_2(k_2-1)\theta_2 + b_1k_2\theta_3 + b_2k_1\theta_3] + \frac{1}{2} [c_1(\tau-k_1-1)\theta_1 \\ &\quad + c_2(n-\tau-k_2-1)\theta_2 + c_1(n-\tau-k_2)\theta_3 + c_2(\tau-k_1)\theta_3] = \beta_1 + \beta_2, \text{ say,} \end{aligned}$$

where $b_1 = k_1/k$, $b_2 = k_2/k = 1 - b_1$, $c_1 = (\tau - k_1)/(n - k)$ and $c_2 = (n - \tau - k_2)/(n - k) = 1 - c_1$. Since $\theta_3 > \max\{\theta_1, \theta_2\}$, for $k_1, k_2 \geq 1$, we have $b_1k_2\theta_3 \geq b_1(k_2-1)\theta_2 + b_1\theta_3$ and $b_2k_1\theta_3 \geq b_2(k_1-1)\theta_1 + b_2\theta_3$. These two inequalities imply $\beta_1 \geq \frac{1}{2}[(k_1-1)\theta_1 + (k_2-1)\theta_2 + \theta_3]$. Similarly, for $\tau - k_1, n - \tau - k_2 \geq 1$, we have $\beta_2 \geq \frac{1}{2}[(\tau - k_1 - 1)\theta_1 + (n - \tau - k_2 - 1)\theta_2 + \theta_3]$. These two together imply

$$\beta_1 + \beta_2 \geq \frac{1}{2}[(\tau-1)\theta_1 + (n-\tau-1)\theta_2 + (2\theta_3 - \theta_1 - \theta_2)] > \frac{1}{2}[(\tau-1)\theta_1 + (n-\tau-1)\theta_2] = \beta_0.$$

So, combining all these cases, for any $S \neq S_\tau, S_\tau^c$, we have $P(\lambda_0(S) > \lambda_0(S_\tau)) \rightarrow 1$ as $d \rightarrow \infty$. Since S_0 is a minimizer of $\lambda_0(S)$, this implies $P((S_0 = S_\tau) \cup (S_0 = S_\tau^c)) \rightarrow 1$ as $d \rightarrow \infty$.

(ii) For a subset $\mathbb{S}_j = \{j\}$ with $j > \tau$, as $d \rightarrow \infty$. we have

$$\begin{aligned} \frac{\lambda_0(\mathbb{S}_j)}{d} &\xrightarrow{P} \frac{1}{2(n-1)} [\tau(\tau-1)\theta_1 + (n-\tau-1)(n-\tau-2)\theta_2 + 2\tau(n-\tau-1)\theta_3] \\ &= \frac{1}{2(n-1)} [\tau(\tau-1)\theta_1 + (n-\tau-1)(n-\tau-2)\theta_2 + \tau(n-\tau-1)(\theta_1 + \theta_2)] \\ &= \frac{1}{2(n-1)} [\tau(n-2)\theta_1 + (n-\tau-1)(n-2)\theta_2] = \frac{1}{2} \left[\left(1 - \frac{1}{n-1}\right) \tau \theta_1 + \left(1 - \frac{1}{n-1}\right) (n-\tau-1) \theta_2 \right] \end{aligned}$$

Now, consider any other subset S with $|S| = k$ where $1 < k < n - 1$. Define k_1 and k_2 as in part (i) of the theorem. For such a subset, it is now easy to check that (replace $2\theta_3$ by $\theta_1 + \theta_2$ in the limiting expression obtained in part(i)) as $d \rightarrow \infty$,

$$\begin{aligned} \frac{\lambda_0(S)}{d} &\xrightarrow{P} \frac{1}{2} \left[\left(1 - \frac{1}{k}\right) k_1 \theta_1 + \left(1 - \frac{1}{k}\right) k_2 \theta_2 + \left(1 - \frac{1}{n-k}\right) (\tau - k_1) \theta_1 + \left(1 - \frac{1}{n-k}\right) (n - \tau - k_2) \theta_2 \right] \\ \implies \frac{\lambda_0(S) - \lambda_0(\mathbb{S}_j)}{d} &\xrightarrow{P} \frac{1}{2} \left[\left(\frac{\tau}{n-1} - \frac{k_1}{k} - \frac{\tau - k_1}{n-k}\right) \theta_1 + \left(\frac{n - \tau - 1}{n-1} + 1 - \frac{k_2}{k} - \frac{n - \tau - k_2}{n-k}\right) \theta_2 \right] \end{aligned}$$

One can check that the coefficient of θ_1 is negative of the coefficient of θ_2 . Hence,

$$\frac{2\{\lambda_0(S) - \lambda_0(\mathbb{S}_j)\}}{d} \xrightarrow{P} \left(\frac{\tau}{n-1} - \frac{k_1}{k} - \frac{\tau - k_1}{n-k}\right) (\theta_1 - \theta_2) = \left(\frac{\tau}{n} + \frac{\tau}{n(n-1)} - \frac{k_1}{k} - \frac{\tau - k_1}{n-k}\right) (\theta_1 - \theta_2).$$

For $k_1 = 0$ or $k_1 = \tau$, it is easy to check that $\frac{\tau}{n-1} - \frac{k_1}{k} - \frac{\tau - k_1}{n-k} < 0$ and hence $\left(\frac{\tau}{n-1} - \frac{k_1}{k} - \frac{\tau - k_1}{n-k}\right) (\theta_1 - \theta_2) > 0$. For $1 < k_1 < \tau$, first note that $\frac{\tau}{n}$ is a weighted average of $\frac{k_1}{k}$ and $\frac{\tau - k_1}{n-k}$. So, we have $\frac{\tau}{n} \leq \max\{\frac{k_1}{k}, \frac{\tau - k_1}{n-k}\}$. Also, $\frac{\tau}{n(n-1)} < \frac{1}{n-1} < \min\{\frac{k_1}{k}, \frac{\tau - k_1}{n-k}\}$ and $\theta_1 - \theta_2 < 0$. So, $P(\lambda_0(S) > \lambda_0(\mathbb{S}_j)) \rightarrow 1$ as $d \rightarrow \infty$.

Again for \mathbb{S}_j with $j \leq \tau$. one can check that

$$\frac{\lambda_0(\mathbb{S}_j)}{d} \xrightarrow{P} \frac{1}{2} \left[\left(1 - \frac{1}{n-1}\right) (\tau - 1) \theta_1 + \left(1 - \frac{1}{n-1}\right) (n - \tau) \theta_2 \right],$$

which is larger than the limiting value of $\lambda_0(\mathbb{S}_j)/d$ for $j > \tau$. This implies that a minimizer of $\lambda_0(S)$ should be of the form \mathbb{S}_j or \mathbb{S}_j^c for some $j > \tau$ with probability tending to 1. \square

Proof of Theorem 1: Under the given condition, for $i, j \leq \tau$ and $i, j > \tau$, $d^{-1/2} \delta_0(\mathbf{X}_i, \mathbf{X}_j)$ converges in probability to 0, but for $i \leq \tau < j$, it converges to a positive constant. So, Lemma 3(i) (replace the Euclidean distance by δ_0) shows that as d grows to infinity, the k -means algorithm leads to two clusters $\{\mathbf{X}_1, \dots, \mathbf{X}_\tau\}$ and $\{\mathbf{X}_{\tau+1}, \dots, \mathbf{X}_n\}$ with probability tending to 1. As a result, $R(\tau) \xrightarrow{P} 0$ and $\mathcal{I}(\tau) \xrightarrow{P} 0$, but for other values of $t \neq \tau$, $R(t)$ and $\mathcal{I}(t)$ converge (in probability) to positive quantities. So, we have $t_R^* \xrightarrow{P} \tau$ and $t_{\mathcal{I}}^* \xrightarrow{P} \tau$, while R_{\min} and \mathcal{I}_{\min} both converge to 0 in probability.

Now, what remains to show is that for both methods, the cut-off values are strictly positive. This will ensure the rejection of \mathcal{H}_0 . We have seen that under permutation, the numbers of observations in two clusters (i.e., numbers of red and blue dots) remain the same, i.e., τ and $n - \tau$. The only difference is that instead of first τ places, red dots are assigned in $\pi(1)$ -th, \dots , $\pi(\tau)$ -th positions. where π is a random permutation of $\{1, 2, \dots, n\}$. Now, note that R_{\min} or \mathcal{I}_{\min} can take the value 0 only when all red dots are followed or preceded by all blue dots. This can happen only in two ways. So, under the permutation distribution (or conditional null distribution), we have $P_{\mathcal{H}_0}(R_{\min} = 0 \mid \tau, n - \tau) = P_{\mathcal{H}_0}(\mathcal{I}_{\min} = 0 \mid \tau, n - \tau) = 2/\binom{n}{\tau}$, which is smaller than α (under the condition given in the theorem). So, the cut-offs are positive in both cases. \square

Lemma 4. $2\sqrt{\mu^2 + \sigma_1^2 + \sigma_2^2} - \sigma_1\sqrt{2} - \sigma_2\sqrt{2} = 0$ if and only if $\mu^2 = 0$ and $\sigma_1^2 = \sigma_2^2$.

Proof: The ‘if’ part is trivial. For the ‘only if’ part, note that

$$\begin{aligned}
& 2\sqrt{\mu^2 + \sigma_1^2 + \sigma_2^2} - \sigma_1\sqrt{2} - \sigma_2\sqrt{2} \\
&= 2\left(\sqrt{\mu^2 + \sigma_1^2 + \sigma_2^2} - \sqrt{\sigma_1^2 + \sigma_2^2}\right) + 2\sqrt{\sigma_1^2 + \sigma_2^2} - \sigma_1\sqrt{2} - \sigma_2\sqrt{2} \\
&= 2\left(\sqrt{\mu^2 + \sigma_1^2 + \sigma_2^2} - \sqrt{\sigma_1^2 + \sigma_2^2}\right) + \sqrt{2}\left(\sqrt{2(\sigma_1^2 + \sigma_2^2)} - (\sigma_1 + \sigma_2)\right) \\
&= 2\left(\sqrt{\mu^2 + \sigma_1^2 + \sigma_2^2} - \sqrt{\sigma_1^2 + \sigma_2^2}\right) + \sqrt{2}\left(\sqrt{(\sigma_1 + \sigma_2)^2 + (\sigma_1 - \sigma_2)^2} - \sqrt{(\sigma_1 + \sigma_2)^2}\right)
\end{aligned}$$

If the sum of these two non-negative terms is 0, each of them must be 0. Now, the first term is 0 if and only if $\mu^2 = 0$, while the second term is 0 if and only if $\sigma_1 = \sigma_2$ or $\sigma_1^2 = \sigma_2^2$. \square

Proof of Theorem 2: For some fixed $i \neq j$, define $Z_d = \frac{1}{d}\|\mathbf{X}_i - \mathbf{X}_j\|^2$. Since $(Z_d - E(Z_d))/\sqrt{\text{Var}(Z_d)} = O_P(1)$, we have $Z_d - E(Z_d) = O_P(v_d/d)$. Now, note that

$$\sqrt{Z_d} - \sqrt{E(Z_d)} = \frac{Z_d - E(Z_d)}{\sqrt{Z_d} + \sqrt{E(Z_d)}} = \frac{Z_d - E(Z_d)}{\sqrt{\text{Var}(Z_d)}} \times \frac{\sqrt{\text{Var}(Z_d)d/v_d}}{\sqrt{Z_d d/v_d} + \sqrt{E(Z_d)d/v_d}}.$$

The first term on the right side is $O_P(1)$. For the second term, we can check that (i) $E(Z_d) = 2 \text{tr}(\boldsymbol{\Sigma}_{1,d})/d$ if $i, j \leq \tau$ (ii) $E(Z_d) = 2 \text{tr}(\boldsymbol{\Sigma}_{2,d})/d$ if $i, j > \tau$ and (iii) $E(Z_d) = \text{tr}(\boldsymbol{\Sigma}_{1,d} + \boldsymbol{\Sigma}_{2,d})/d + \|\boldsymbol{\mu}_{1,d} - \boldsymbol{\mu}_{2,d}\|^2/d$ if $i < \tau < j$ or $j < \tau < i$. So, in all these cases, $E(Z_d)d \geq 2 \min\{\text{tr}(\boldsymbol{\Sigma}_{1,d}), \text{tr}(\boldsymbol{\Sigma}_{2,d})\}$. Since $\lim_{d \rightarrow \infty} \min\{\text{tr}(\boldsymbol{\Sigma}_{1,d}), \text{tr}(\boldsymbol{\Sigma}_{2,d})\}/v_d > 0$, $E(Z_d)d/v_d$ remains bounded away from 0. Hence, $\sqrt{Z_d d/v_d} + \sqrt{E(Z_d)d/v_d}$ also remains bounded away from zero or $1/(\sqrt{Z_d d/v_d} + \sqrt{E(Z_d)d/v_d})$ remains bounded away from infinity with probability 1. Or in other words, we have $1/(\sqrt{Z_d d/v_d} + \sqrt{E(Z_d)d/v_d}) = O_P(1)$. Again, $\sqrt{\text{Var}(Z_d)d/v_d} = O(\sqrt{v_d/d})$. So, combining all these things, we get $\sqrt{Z_d} = \sqrt{E(Z_d)} + O_P(\sqrt{v_d/d})$, i.e., $d^{-1/2}\|\mathbf{X}_i - \mathbf{X}_j\| = d^{-1/2}\sqrt{E(\|\mathbf{X}_i - \mathbf{X}_j\|^2)} + O_P(\sqrt{v_d/d})$.

In addition to \mathbf{X}_i and \mathbf{X}_j , if we also consider \mathbf{X}_k for some $k \neq i, j$, we have

$$d^{-1/2}\left|\|\mathbf{X}_i - \mathbf{X}_k\| - \|\mathbf{X}_j - \mathbf{X}_k\|\right| = d^{-1/2}\left|\sqrt{E(\|\mathbf{X}_i - \mathbf{X}_k\|^2)} - \sqrt{E(\|\mathbf{X}_j - \mathbf{X}_k\|^2)}\right| + O_P(\sqrt{v_d/d}).$$

Since this holds for all $i \neq j \neq k$ ($1 \leq i, j, k \leq n$) and the sample size n is finite, this implies $d^{-1/2}\delta_0(\mathbf{X}_i, \mathbf{X}_j) = O_P(\sqrt{v_d/d})$ or $v_d^{-1/2}\delta_0(\mathbf{X}_i, \mathbf{X}_j) = O_P(1)$ for all $i, j \leq \tau$ and $i, j > \tau$. However, for $i \leq \tau < j$ or $j \leq \tau < i$, we have $v_d^{-1/2}\delta_0(\mathbf{X}_i, \mathbf{X}_j) = v_d^{-1/2}\delta_0^*(F_1, F_2) + O_P(1)$, where

$$\begin{aligned}
\delta_0^*(F_1, F_2) &= \frac{1}{n-2}\left[(\tau-1)\left|\sqrt{\|\boldsymbol{\mu}_{1,d} - \boldsymbol{\mu}_{2,d}\|^2 + \text{tr}(\boldsymbol{\Sigma}_{1,d}) + \text{tr}(\boldsymbol{\Sigma}_{2,d})} - \sqrt{2\text{tr}\{\boldsymbol{\Sigma}_{1,d}\}}\right|\right. \\
&\quad \left.+ (n-\tau-1)\left|\sqrt{\|\boldsymbol{\mu}_{1,d} - \boldsymbol{\mu}_{2,d}\|^2 + \text{tr}(\boldsymbol{\Sigma}_{1,d}) + \text{tr}(\boldsymbol{\Sigma}_{2,d})} - \sqrt{2\text{tr}\{\boldsymbol{\Sigma}_{2,d}\}}\right|\right].
\end{aligned}$$

For $1 < \tau < n-1$, since, $(n-2)\delta_0^*(F_1, F_2) \geq 2\sqrt{\|\boldsymbol{\mu}_{1,d} - \boldsymbol{\mu}_{2,d}\|^2 + \text{tr}(\boldsymbol{\Sigma}_{1,d}) + \text{tr}(\boldsymbol{\Sigma}_{2,d})} - \sqrt{2\text{tr}\{\boldsymbol{\Sigma}_{1,d}\}} - \sqrt{2\text{tr}\{\boldsymbol{\Sigma}_{2,d}\}}$, from the proof of Lemma 4, it is easy to see that under the given condition $v_d^{-1/2}\delta_0^*(F_1, F_2)$ diverges to infinity as d increases. So, for $i, j \leq \tau$ or $i, j > \tau$ while $v_d^{-1/2}\delta_0(\mathbf{X}_i, \mathbf{X}_j)$ remains bounded

in probability, for $i \leq \tau < j$ or $j \leq \tau < i$, we have $P(v_d^{-1/2} \delta_0(\mathbf{X}_i, \mathbf{X}_j) > M) \rightarrow 1$ for any large M . As a result, $\lambda^*(C_1, C_2)$ is minimized when $\mathbf{X}_1, \dots, \mathbf{X}_\tau$ are in one cluster and $\mathbf{X}_{\tau+1}, \dots, \mathbf{X}_n$ in the other (see Lemma 3(i)). So, while $R(\tau) \xrightarrow{P} 0$ and $\mathcal{I}(\tau) \xrightarrow{P} 0$, for other values of $t \neq \tau$ ($t = 1, 2, \dots, n-1$), we have $P(R(t) > 0) \rightarrow 1$ and $P(\mathcal{I}(t) > 0) \rightarrow 1$. As a consequence, (i) $P(t_0^R = \tau)$ and $P(t_0^{\mathcal{I}} = \tau)$ both converge to 1 and (ii) R_{\min} and \mathcal{I}_{\min} both converge to 0 in probability. The rest of the proof follows from the argument involving permutation distribution used in the proof of Theorem 1. \square

Proof of Theorem 3: Under (A2), using the uniform continuity of h , we have $|\rho_{h,\psi}(\mathbf{X}_i, \mathbf{X}_j) - h(\tilde{\theta}_{\psi,1,d})| \xrightarrow{P} 0$ for $i, j \leq \tau$, $|\rho_{h,\psi}(\mathbf{X}_i, \mathbf{X}_j) - h(\tilde{\theta}_{\psi,2,d})| \xrightarrow{P} 0$ for $i, j > \tau$ and $|\rho_{h,\psi}(\mathbf{X}_i, \mathbf{X}_j) - h(\tilde{\theta}_{\psi,3,d})| \xrightarrow{P} 0$ for $i \leq \tau < j$. Now, consider the case $i \leq \tau < j$. Using the inequality $|a| - |b| \leq |a - b|$, for any $k \leq \tau$ ($k \neq i$), we get $|\rho_{h,\psi}(\mathbf{X}_i, \mathbf{X}_k) - \rho_{h,\psi}(\mathbf{X}_j, \mathbf{X}_k)| - |h(\tilde{\theta}_{\psi,1,d}) - h(\tilde{\theta}_{\psi,3,d})| \xrightarrow{P} 0$. Similarly, for any $k > \tau$ ($k \neq j$), we have $|\rho_{h,\psi}(\mathbf{X}_i, \mathbf{X}_k) - \rho_{h,\psi}(\mathbf{X}_j, \mathbf{X}_k)| - |h(\tilde{\theta}_{\psi,3,d}) - h(\tilde{\theta}_{\psi,2,d})| \xrightarrow{P} 0$. These two results together imply that $|\delta_{h,\psi}(\mathbf{X}_i, \mathbf{X}_j) - \tilde{\delta}_{h,\psi,d}| \xrightarrow{P} 0$, where

$$\begin{aligned} (n-2) \tilde{\delta}_{h,\psi,d} &= (\tau-1) |h(\tilde{\theta}_{\psi,1,d}) - h(\tilde{\theta}_{\psi,3,d})| + (n-\tau-1) |h(\tilde{\theta}_{\psi,3,d}) - h(\tilde{\theta}_{\psi,2,d})| \\ &\geq |h(\tilde{\theta}_{\psi,1,d}) - h(\tilde{\theta}_{\psi,3,d})| + |h(\tilde{\theta}_{\psi,3,d}) - h(\tilde{\theta}_{\psi,2,d})| \\ &\geq 2h(\tilde{\theta}_{\psi,3,d}) - h(\tilde{\theta}_{\psi,1,d}) - h(\tilde{\theta}_{\psi,2,d}). \end{aligned}$$

Now, $\bar{\mathcal{E}}_{\psi,d} > 0 \implies \tilde{\theta}_{\psi,3,d} \geq \frac{1}{2}(\tilde{\theta}_{\psi,1,d} + \tilde{\theta}_{\psi,2,d})$. Since h is concave and monotonically increasing, this further implies $h(\tilde{\theta}_{\psi,3,d}) > h\left(\frac{1}{2}\tilde{\theta}_{\psi,1,d} + \frac{1}{2}\tilde{\theta}_{\psi,2,d}\right) \geq \frac{1}{2}h(\tilde{\theta}_{\psi,1,d}) + \frac{1}{2}h(\tilde{\theta}_{\psi,2,d})$.

So, $\liminf_{d \rightarrow \infty} \bar{\mathcal{E}}_{\psi,d} > 0$ implies $\tilde{\delta}_{h,\psi,d}$ (and hence $\delta_{h,\psi}(\mathbf{X}_i, \mathbf{X}_j)$) remains bounded away from 0. On the other hand, for $i, j \leq \tau$ or $i, j > \tau$, one can show that $\delta_{h,\psi}(\mathbf{X}_i, \mathbf{X}_j) \xrightarrow{P} 0$. Therefore, following part (i) of Lemma 3, the k -means clustering algorithm based on $\delta_{h,\psi}$ leads to two clusters $\{\mathbf{X}_1, \dots, \mathbf{X}_\tau\}$ and $\{\mathbf{X}_{\tau+1}, \dots, \mathbf{X}_n\}$. The rest of argument is the same as that used in the proof of Theorem 1. \square

Proof of Theorem 4: For some fixed $i \neq j$, define $Z_{\psi,d} = \frac{1}{d} \sum_{q=1}^d \psi\left(|\mathbf{X}_i^{(q)} - \mathbf{X}_j^{(q)}|^2\right)$. Since $(Z_{\psi,d} - E(Z_{\psi,d}))/\sqrt{\text{Var}(Z_{\psi,d})} = O_P(1)$, we have $Z_{\psi,d} - E(Z_{\psi,d}) = O_P(v_{\psi,d}/d)$. Now, $|h(Z_{\psi,d}) - h(E(Z_{\psi,d}))| \leq C|Z_{\psi,d} - E(Z_{\psi,d})|$ (note that h is Lipschitz continuous), where C is a constant. So, $|\rho_{h,\psi}(\mathbf{X}_i, \mathbf{X}_j) - h(E(Z_{\psi,d}))| = O_P(v_{\psi,d}/d)$.

Therefore, for $i, j \leq \tau$, we get $\rho_{h,\psi}(\mathbf{X}_i, \mathbf{X}_j) = h\left(\frac{1}{d} \sum_{q=1}^d \theta_{\psi,1}(q)\right) + O_P(v_{\psi,d}/d)$. Similarly, we have $\rho_{h,\psi}(\mathbf{X}_i, \mathbf{X}_j) = h\left(\frac{1}{d} \sum_{q=1}^d \theta_{\psi,2}(q)\right) + O_P(v_{\psi,d}/d)$ for $i, j > \tau$ and $\rho_{h,\psi}(\mathbf{X}_i, \mathbf{X}_j) = h\left(\frac{1}{d} \sum_{q=1}^d \theta_{\psi,3}(q)\right) + O_P(v_{\psi,d}/d)$ for $i \leq \tau < j$. This implies that (i) for $i, j \leq \tau$ and $i, j > \tau$, $\delta_{h,\psi}(\mathbf{X}_i, \mathbf{X}_j) = O_P(v_{\psi,d}/d)$ and (ii) for $i \leq \tau < j$, $\delta_{h,\psi}(\mathbf{X}_i, \mathbf{X}_j) = \tilde{\delta}_{h,\psi,d} + O_P(v_{\psi,d}/d)$. So, for $i, j \leq \tau$ or $i, j > \tau$ while $\delta_{h,\psi}(\mathbf{X}_i, \mathbf{X}_j)d/v_{\psi,d}$ remains bounded in probability, for $i \leq \tau < j$, it diverges to infinity (since $\tilde{\delta}_{h,\psi,d} d/v_{\psi,d} \rightarrow \infty$ as $d \rightarrow \infty$). The rest of the proof follows using the same argument as in the proof of Theorem 2. \square

References

- Ahn, J., Lee, M. H., and Yoon, Y. J. (2012). Clustering high dimension, low sample size data using the maximal data piling distance. *Statist. Sinica*, 22(2):443–464.
- Alcock, R. J. and Manolopoulos, Y. (1999). Time-series similarity queries employing a feature-based approach. In *7th Hellenic Conference on Informatics, Ioannina*, pages 27–29.
- Arlot, S., Celisse, A., and Harchaoui, Z. (2019). A kernel multiple change-point algorithm via model selection. *J. Mach. Learn. Res.*, 20(162):1–56.
- Aryal, S., Ting, K.-M., Washio, T., and Haffari, G. (2017). Data-dependent dissimilarity measure: an effective alternative to geometric distance measures. *Knowledge and Information Systems*, 53(2):479–506.
- Aston, J. and Kirch, C. (2014). Change points in high dimensional settings. *ArXiv preprint arXiv:1409.1771*, pages 1–34.
- Aue, A., Hörmann, S., Horváth, L., and Reimherr, M. (2009). Break detection in the covariance structure of multivariate time series models. *Ann. Statist.*, 37(6B):4046–4087.
- Avanesov, V. and Buzun, N. (2018). Change-point detection in high-dimensional covariance structure. *Electron. J. Stat.*, 12(2):3254–3294.
- Baringhaus, L. and Franz, C. (2010). Rigid motion invariant two-sample tests. *Statist. Sinica*, 20(4):1333–1361.
- Bhattacharyya, G. K. and Johnson, R. A. (1968). Nonparametric tests for shift at an unknown time point. *Ann. Math. Statist.*, 39(5):1731–1743.
- Borysov, P., Hannig, J., and Marron, J. S. (2014). Asymptotics of hierarchical clustering for growing dimension. *J. Multivariate Analysis*, 124:465–479.
- Breiman, L., Friedman, J., Stone, C. J., and Olshen, R. A. (1984). *Classification and Regression Trees*. CRC Press, Boca Raton, Florida.
- Brodsky, E. and Darkhovsky, B. S. (2013). *Nonparametric Methods in Change-Point Problems*, volume 243. Kluwer Academic Publishers, Dordrecht.
- Carlstein, E. (1988). Nonparametric change-point estimation. *Ann. Statist.*, 16(1):188–197.
- Chen, H. and Zhang, N. (2015). Graph-based change-point detection. *Ann. Statist.*, 43(1):139–176.
- Chen, J. and Gupta, A. K. (1997). Testing and locating variance changepoints with application to stock prices. *J. Amer. Statist. Assoc.*, 92(438):739–747.
- Chen, J. and Gupta, A. K. (1999). Change point analysis of a gaussian model. *Statist. Papers*, 40(3):323–333.
- Chen, J. and Gupta, A. K. (2011). *Parametric Statistical Change Point Analysis: With Applications to Genetics, Medicine, and Finance*. Birkhauser, Boston.
- Cox, D. R. and Spjøtvoll, E. (1982). On partitioning means into groups. *Scand. J. Stat.*, 9(3):147–152.

- Csörgő, M. and Horváth, L. (1987). Nonparametric tests for the change-point problem. *J. Statist. Plann. Inference*, 17:1–9.
- Desobry, F., Davy, M., and Doncarli, C. (2005). An online kernel change detection algorithm. *IEEE Trans. Signal Process.*, 53(8):2961–2974.
- Eagle, N. and Pentland, A. S. (2006). Reality mining: sensing complex social systems. *Personal and Ubiquitous Computing*, 10(4):255–268.
- Elhamifar, E. and Vidal, R. (2013). Sparse subspace clustering: Algorithm, theory, and applications. *IEEE Trans. Pattern Anal. Mach. Intell.*, 35(11):2765–2781.
- Francois, D., Wertz, V., and Verleysen, M. (2007). The concentration of fractional distances. *IEEE Trans. Knowl. Data Eng.*, 19(7):873–886.
- Friedman, J. H., Hastie, T., and Tibshirani, R. (2001). *The Elements of Statistical Learning*, volume 1. Springer series in statistics New York.
- Friedman, J. H. and Rafsky, L. C. (1979). Multivariate generalizations of the Wald-Wolfowitz and Smirnov two-sample tests. *Ann. Statist.*, 7(4):697–717.
- Girshick, M. A. and Rubin, H. (1952). A Bayes approach to a quality control model. *Ann. Math. Statist.*, 23(1):114–125.
- Hall, P., Marron, J. S., and Neeman, A. (2005). Geometric representation of high dimension, low sample size data. *J. R. Stat. Soc. Ser. B. Stat. Methodol.*, 67(3):427–444.
- Harchaoui, Z., Moulines, E., and Bach, F. (2008). Kernel change-point analysis. *Adv. Neural Info. Process. Sys.*, 21:609–616.
- Henze, N. (1988). A multivariate two-sample test based on the number of nearest neighbor type coincidences. *Ann. Statist.*, 16(2):772–783.
- James, B., James, K. L., and Siegmund, D. (1987). Tests for a change-point. *Biometrika*, 74(1):71–83.
- James, B., James, K. L., and Siegmund, D. (1992). Asymptotic approximations for likelihood ratio tests and confidence regions for a change-point in the mean of a multivariate normal distribution. *Statist. Sinica*, 2(1):69–90.
- Jung, S. and Marron, J. S. (2009). PCA consistency in high dimension, low sample size context. *Ann. Statist.*, 37(6B):4104–4130.
- Kundu, D. (2014). Geometric skew normal distribution. *Sankhyā B*, 76(2):167–189.
- Lee, C.-B. (1995). Estimating the number of change points in a sequence of independent normal random variables. *Statist. Probab. Lett.*, 25(3):241–248.
- Li, S., Xie, Y., Dai, H., and Song, L. (2015). M-statistic for kernel change-point detection. In *Adv. in Neural Info. Process. Sys.*, pages 3366–3374.

- Lu, B., Greevy, R., Xu, X., and Beck, C. (2011). Optimal non-bipartite matching and its statistical applications. *Amer. Statist.*, 65(1):21–30.
- Lung-Yut-Fong, A., Lévy-Leduc, C., and Cappé, O. (2015). Homogeneity and change-point detection tests for multivariate data using rank statistics. *Journal de la Société Française de Statistique*, 156(4):133–162.
- Matteson, D. S. and James, N. A. (2014). A nonparametric approach for multiple change point analysis of multivariate data. *J. Amer. Statist. Assoc.*, 109(505):334–345.
- Page, E. S. (1954). Continuous inspection schemes. *Biometrika*, 41(1/2):100–115.
- Page, E. S. (1955). A test for a change in a parameter occurring at an unknown point. *Biometrika*, 42(3/4):523–527.
- Page, E. S. (1957). On problems in which a change in a parameter occurs at an unknown point. *Biometrika*, 44(1/2):248–252.
- Pal, A. K., Mondal, P. K., and Ghosh, A. K. (2016). High dimensional nearest neighbor classification based on mean absolute differences of inter-point distances. *Pattern Recognit. Lett.*, 74:1–8.
- Pettitt, A. N. (1979). A non-parametric approach to the change-point problem. *J. R. Stat. Soc. Ser. C. Appl. Stat.*, 28(2):126–135.
- Radovanovic, M., Nanopoulos, A., and Ivanovic, M. (2010). Hubs in space: popular nearest neighbors in high-dimensional data. *J. Mach. Learn. Res.*, 11:2487–2531.
- Rand, W. M. (1971). Objective criteria for the evaluation of clustering methods. *J. Amer. Statist. Assoc.*, 66(336):846–850.
- Rosenbaum, P. R. (2005). An exact distribution-free test comparing two multivariate distributions based on adjacency. *J. R. Stat. Soc. Ser. B. Stat. Methodol.*, 67(4):515–530.
- Roy, A., Ghosh, A. K., Goswami, A., and Murthy, C. (2020). Some new copula based distribution-free tests of independence among several random variables. *Sankhya A*, pages 1–41.
- Sarkar, S. and Ghosh, A. K. (2020). On perfect clustering of high dimension, low sample size data. *IEEE Trans. Pattern Anal. Mach. Intell.*, 43(9):2257–2272.
- Schilling, M. F. (1986). Multivariate two-sample tests based on nearest neighbors. *J. Amer. Statist. Assoc.*, 81(395):799–806.
- Sen, A. K. and Srivastava, M. S. (1973). On multivariate tests for detecting change in mean. *Sankhyā A*, 35(2):173–186.
- Sen, A. K. and Srivastava, M. S. (1975). On tests for detecting change in mean. *Ann. Statist.*, 3(1):98–108.
- Shao, X. and Zhang, X. (2010). Testing for change points in time series. *J. Amer. Statist. Assoc.*, 105(491):1228–1240.
- Shi, X., Wu, Y., and Rao, C. R. (2017). Consistent and powerful graph-based change-point test for high-dimensional data. *Proc. Natl. Acad. Sci. USA*, 114(15):3873–3878.

- Siegmund, D., Yakir, B., and Zhang, N. R. (2011). Detecting simultaneous variant intervals in aligned sequences. *Ann. Appl. Statist.*, 5(2A):645–668.
- Srivastava, M. S. and Worsley, K. J. (1986). Likelihood ratio tests for a change in the multivariate normal mean. *J. Amer. Statist. Assoc.*, 81(393):199–204.
- Sun, Y.-W., Papagiannouli, K., and Spokoiny, V. (2019). Online graph-based change-point detection for high dimensional data. *arXiv preprint arXiv:1906.03001*.
- Székely, G. J. and Rizzo, M. L. (2013). Energy statistics: A class of statistics based on distances. *J. Statist. Plann. Inference*, 143(8):1249–1272.
- Székely, G. J., Rizzo, M. L., and Bakirov, N. K. (2007). Measuring and testing dependence by correlation of distances. *Ann. Statist.*, 35(6):2769–2794.
- Ting, K.-M., Zhu, Y., Carman, M., Zhu, Y., and Zhou, Z.-H. (2016). Overcoming key weaknesses of distance-based neighbourhood methods using a data dependent dissimilarity measure. In *Proceedings of the 22nd ACM SIGKDD International Conference on Knowledge Discovery and Data Mining*, pages 1205–1214.
- Wang, D., Yu, Y., and Rinaldo, A. (2021). Optimal covariance change point localization in high dimension. *Bernoulli*, 27(1):554–575.
- Wang, T. and Samworth, R. J. (2018). High dimensional change point estimation via sparse projection. *J. R. Stat. Soc. Ser. B. Stat. Methodol.*, 80(1):57–83.
- Wolfe, D. A. and Schechtman, E. (1984). Nonparametric statistical procedures for the change-point problem. *J. Statist. Plann. Inference*, 9(3):389–396.
- Worsley, K. J. (1986). Confidence regions and tests for a change-point in a sequence of exponential family random variables. *Biometrika*, 73(1):91–104.
- Yao, Y.-C. (1988). Estimating the number of change points via Schwarz’ criterion. *Statist. Probab. Lett.*, 6(3):181–189.
- Zhang, N. R., Siegmund, D., Ji, H., and Li, J. Z. (2010). Detecting simultaneous change-points in multiple sequences. *Biometrika*, 97(3):631–645.
- Zou, C., Yin, G., Feng, L., and Wang, Z. (2014). Nonparametric maximum likelihood approach to multiple change-point problems. *Ann. Statist.*, 42(3):970–1002.